hydrogen

MDPI

Article

The Boundary between Two Modes of Gas Evolution: Oscillatory (H_2 and O_2) and Conventional Redox (O_2 Only), in the Hydrocarbon/H_2O_2/Cu(II)/CH_3CN System

Igor Yu. Shchapin [1,2,*] and Andrey I. Nekhaev [3]

[1] Scientific Research Institute of Space Device Engineering, Aviamotornaya Street 53, 111024 Moscow, Russia
[2] Department of High Energy Chemistry and Radioecology, D.I. Mendeleev University of Chemical Technology of Russia, Miusskaya Ploshchad 9, 125047 Moscow, Russia
[3] A.V. Topchiev Institute of Petrochemical Synthesis, Russian Academy of Sciences, Leninsky Prospect 29, 119991 Moscow, Russia
* Correspondence: shchapin@yandex.ru

Abstract: During the oxidation of hydrocarbons using hydrogen peroxide solutions, the evolution of gaseous oxygen is a side and undesirable process, in which the consumption of the oxidizer is not associated with the formation of target products. Therefore, no attention is paid to the systematic study of the chemical composition of the gas and the mechanisms of its formation. Filling this gap, the authors discovered a number of new, previously unidentified, interesting facts concerning both gas evolution and the oxidation of hydrocarbons. In a 33% $H_2O_2/Cu_2Cl_4{\cdot}2DMG/CH_3CN$ system, where DMG is dimethylglyoxime (Butane-2,3-dione dioxime), and is at 50 °C, evidence of significant evolution of gaseous hydrogen, along with the evolution of gaseous oxygen was found. In the authors' opinion, which requires additional verification, the ratio of gaseous hydrogen and oxygen in the discussed catalytic system can reach up to 1:1. The conditions in which only gaseous oxygen is formed are selected. Using a number of oxidizable hydrocarbons with the first adiabatic ionization potentials (AIPs) of a wide range of values, it was found that the first stage of such a process of evolving only gaseous oxygen was the single electron transfer from hydrogen peroxide molecules to trinuclear copper clusters with the formation, respectively, of hydrogen peroxide radical cations $H_2O_2^{\bullet+}$ and radical anions $Cu_3Cl_5^{\bullet-}$ (AIP = 5 eV). When the conditions for the implementation of such a single electron transfer mechanism are exhausted, the channel of decomposition of hydrogen peroxide molecules into gaseous hydrogen and oxygen is switched on, which is accompanied by the transition of the system to an oscillatory mode of gas evolution. In some cases, the formation of additional amounts of gaseous products is provided by the catalytically activated decomposition of water molecules into hydrogen and oxygen after the complete consumption of hydrogen peroxide molecules in the reaction of gaseous oxygen evolution. The adiabatic electron affinity of various forms of copper molecules involved in chemical processes is calculated by the density functional theory method.

Keywords: hydrogen and oxygen; gas evolution; oscillatory reaction; hydrogen peroxide; copper chloride; dimethylglyoxime; acetonitrile; ionization potential; electron affinity; DFT calculations

Citation: Shchapin, I.Y.; Nekhaev, A.I. The Boundary between Two Modes of Gas Evolution: Oscillatory (H_2 and O_2) and Conventional Redox (O_2 Only), in the Hydrocarbon/H_2O_2/Cu(II)/CH_3CN System. *Hydrogen* **2023**, *4*, 74–102. https://doi.org/10.3390/hydrogen4010006

Academic Editor: Aleksey A. Vedyagin

Received: 27 November 2022
Revised: 25 December 2022
Accepted: 26 December 2022
Published: 16 January 2023

1. Introduction

In various ways, the initiated transitions of hydrogen from a free (molecular) to a bound (as part of chemical compounds) state in the forward and reverse directions have great practical, theoretical, and educational applications [1–4]. It is difficult to find any field of chemistry, in which experimental and theoretical data on the properties and structure of the hydrogen atom and molecule in neutral and ionic forms are not used explicitly or indirectly.

Since hydrogen is the simplest chemical element (ordinal number 1), its atom and molecule in neutral and ionic forms provide chemists with the simplest and most convenient models for describing the structure and chemical behavior of substances consisting of more complex atoms of other elements.

This work is devoted to the study of the features of gas evolution during the decomposition of hydrogen peroxide (H_2O_2) in the presence of catalytic amounts of copper(II) ions. If one compares the processes 1–6 of binding and evolution of gases–hydrogen (H_2) and oxygen (O_2) molecules by thermal effects estimated by the dissociation (formation) energies of chemical bonds of molecules H_2 (4.52 eV [5]), O_2 (5.16 eV [6]), H_2O ($2 \times 5.15 = 10.30$ eV [7]) and H_2O_2 ($2 \times 3.79 + 2.18 = 9.76$ eV [8,9]) (the recommended values from [10], 1 eV = 23.0605 kcal/mol = 96.4905 kJ/mol), then three groups of processes can be distinguished: strongly exothermic (reactions 1 and 5), close to isothermic (reactions 3 and 4), and strongly endothermic (reactions 2 and 6).

$$H_2 + 0.5O_2 \rightarrow H_2O \ (+3.20 \text{ eV}) \quad (1)$$

$$H_2O \rightarrow H_2 + 0.5O_2 \ (-3.20 \text{ eV}) \quad (2)$$

$$H_2 + O_2 \rightarrow H_2O_2 \ (+0.08 \text{ eV}) \quad (3)$$

$$H_2O_2 \rightarrow H_2 + O_2 \ (-0.08 \text{ eV}) \quad (4)$$

$$H_2O_2 \rightarrow H_2O + 0.5O_2 \ (+3.12 \text{ eV}) \quad (5)$$

$$H_2O + 0.5O_2 \rightarrow H_2O_2 \ (-3.12 \text{ eV}) \quad (6)$$

Reactions 1 and 2, 3 and 4, and 5 and 6 are pairs of the same processes that proceed in the forward and reverse directions and, with the exception of reaction 4, are technically implemented as processes proceeding in the same desired direction.

Reaction 1 is widely used in fuel cells and occurs spontaneously [11–14]. Reaction 2 does not occur spontaneously and requires an external energy source, which uses electricity and/or light [15–17].

Reaction 3 proceeds spontaneously on palladium catalysts, individual and in the form of alloys with gold and other metals [18–20]. The role of the catalyst is to convert molecular hydrogen into the atomic form, which initiates a sequence of free radical-like reactions occurring with molecules and particles adsorbed on its surface [21–24]. The proximity of the thermal effect of reaction 3 to zero promotes this type of initiation and flow. Recent advances in the direct synthesis of H_2O_2 (reaction 3) using chemical catalysis are collected in the review [25].

The authors have not been able to find works that describe reaction 4 as an object of research or as a way to implement any technical task. Therefore, reaction 4, which is unusual and not previously explored, is highlighted in red. In this study, signs of unusual reaction 4 were found, which, for methodological reasons, the authors tried to discard.

With catalytic and other methods of decomposition of hydrogen peroxide, the processes of the formation of gas–molecular oxygen by reaction 5 are usually detailed [26–30]. In this work, a lot of attention is paid to reaction 5, since it evolves the minimum possible amount of gas compared to other processes 2 and 4, in which molecular hydrogen is additionally evolved.

Reaction 6 does not occur spontaneously; it requires an external energy source, from which electricity is used [31–33].

Although reaction 4 appears uncommon, it can be considered as the combined effect of the sequential flow of two more familiar reactions 5 and 2.

At the same time, in the case of the catalytically activated most familiar reaction 5, which many authors have studied numerous times and from different angles, there are unresolved problems associated with its first stage–its initiation.

The interaction of transition metal ions with hydrogen peroxide molecules belongs to the class of redox reactions, during which a single electron is transferred between reacting components (SET mechanism).

By analogy with the Fenton system (H_2O_2 + Fe(III)/Fe(II) [34–36]) for other transition metal ions ($M^{n+}/M^{(n-1)+}$ [37]), including copper (reactions 7 and 8) [37,38], cyclic mutual transformations of two forms of metal (oxidized and reduced) with hydrogen peroxide molecules, which respectively act as a reducing agent and oxidizer, are assumed.

As a result, radical ($HO_2^{\bullet}$ and $HO^{\bullet}$) and ionic (H^+ and OH^-) particles are generated, which then react with each other (reactions 9 and 10), giving the final products (O_2 and H_2O) reactions 5. Reaction 9 is the shortest path of radical transformation, leading to O_2 and H_2O, which are usually replaced by sequences of more complex and multi-stage reactions [38,39]. Some authors suggest that intermediate products with Cu–O bonds ($CuOOH^+$ and $CuOH^{2+}$) are formed in reactions 7 and 8 [40,41].

$$Cu^{2+} + H_2O_2 \rightarrow Cu^+ + HO_2^{\bullet} + H^+ \quad (7)$$

$$Cu^+ + H_2O_2 \rightarrow Cu^{2+} + HO^{\bullet} + OH^- \quad (8)$$

$$HO_2^{\bullet} + HO^{\bullet} \rightarrow O_2 + H_2O \quad (9)$$

$$H^+ + OH^- \rightarrow H_2O \quad (10)$$

The unsolved problem is that instead of the sequence of reactions 11–14, in which hydrogen peroxide ion radicals (radical cation $H_2O_2^{\bullet+}$ and radical anion $H_2O_2^{\bullet-}$) should participate, the total reactions 7 and 8 are usually recorded [38,39].

$$Cu^{2+} + H_2O_2 \rightarrow Cu^+ + H_2O_2^{\bullet+} \quad (11)$$

$$H_2O_2^{\bullet+} \rightarrow HO_2^{\bullet} + H^+ \quad (12)$$

$$Cu^+ + H_2O_2 \rightarrow Cu^{2+} + H_2O_2^{\bullet-} \quad (13)$$

$$H_2O_2^{\bullet-} \rightarrow HO^{\bullet} + OH^- \quad (14)$$

The reasons why they do this are not discussed. In the authors' opinion, the main reason for such a simplified approach is that during catalytic transformations, the formation of hydrogen peroxide ion radicals has not yet been registered using physicochemical methods.

This work provides experimental evidence that reaction 11 really occurs in the discussed $RH/H_2O_2/Cu_2Cl_4{\cdot}2DMG/CH_3CN$ catalytic system, where RH is a set of hydrocarbons with the first adiabatic ionization potentials (AIPs, eV) of a wide range, and DMG is dimethylglyoxime (Butane-2,3-dione dioxime).

The structures of all the main components of the above-mentioned catalytic system, including DMG, are shown in Scheme 1: $Cu_2Cl_4{\cdot}2DMG$ catalyst (**1**), an oxidizing mixture consisting of a 33% solution of hydrogen peroxide (**2**) in water (**3**) and a solvent–acetonitrile (**4**), hydrocarbons (RHs): adamantane (**5**), camphor (**6**), o-xylene (**7**), alpha-pinan (**8**), naphthalene (**9**), 2-methyl-naphthalene (**10**).

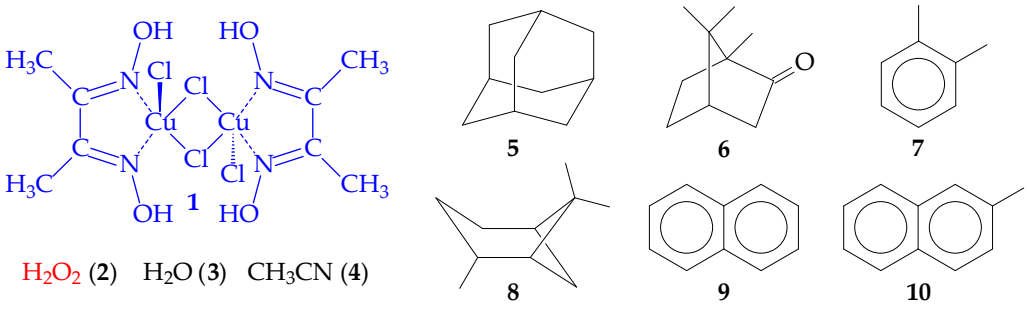

Scheme 1. The catalytic complex $Cu_2Cl_4{\cdot}2DMG$ (**1**) and other components of the reaction mixture.

The catalytic system studied in this work, the components of which are shown in Scheme 1, at 50 °C, with a drip introduction of an oxidizer solution for an hour, is capable of deeply oxidizing RH **5** to pentaols [42].

With a rapid (~3 s) introduction of the oxidizer solution, a mixture of mono- and dioxygenated RH **5** products were mainly formed. The oxidation of RH **5** occurred during the initial reaction period with the participation of catalyst **1**, less than 5 min after mixing of the reagents, before the start of intensive gas evolution, presumably O_2 [42].

Under these conditions, ten hydrocarbons were oxidized with less catalytic activity, but with a selectivity of RH **5** oxidation more similar to that in the Fenton reaction [42]. It was found that under these conditions at a rapid (~3 s) method of introducing the oxidizer solution, the conversion of hydrocarbons varied widely: from 6 to 51%, which indicated great instability of the catalytic system [42].

Under the same conditions, cyclohexane (**11**), Scheme 2, was oxidized with a conversion of 100%, but in the mode of drip introduction of an oxidizer solution [42]. It was concluded that there was an unaccounted factor in the system associated with gas evolution, which strongly influenced the conversion of hydrocarbons [42].

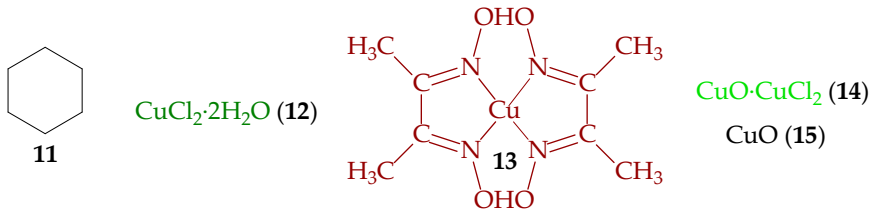

Scheme 2. Additional components of the catalytic system: hydrocarbon **11** and catalysts **12**–**15**.

To overcome the consequences of a large spread in the values of hydrocarbon conversions, a new method of systematization of data on the composition of hydrocarbon oxidation products—the distributive oxidation depth D(O) (Figure 1A) was created, which did not take into account the conversion of hydrocarbons and at the same time had useful analytical properties [43].

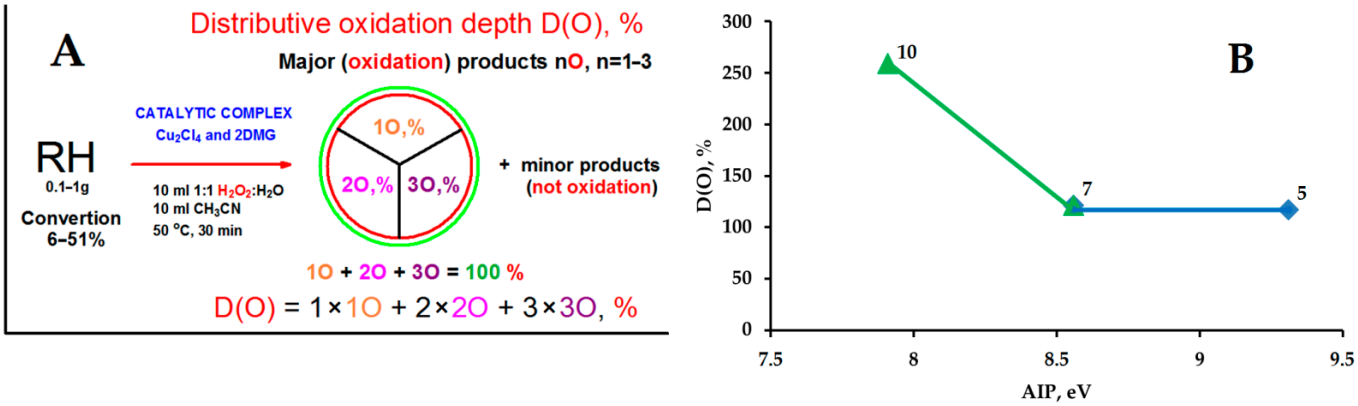

Figure 1. (**A**) The distributive oxidation depth D(O); (**B**) Three characteristic points (RH **5**, **7**, and **10**) on the dependence of D(O) on AIP–the first adiabatic ionization potentials of hydrocarbons RH. Equations of straight lines **y = ax + b**: blue: D(O) = 117 %; green: D(O) = −221.55AIP + 2012 [43].

When comparing D(O) and AIP hydrocarbons, it was useful for the systematization of data related to the selectivity of oxidation of hydrocarbons of different structures: bicyclic, framework, and aromatic. Figure 1B shows two extremes (RH **5** and **10**) and central (RH **7**) points of two linear dependencies that intersect at the AIP(DMG) point and indicate the participation in the oxidation of hydrocarbons of the component (DMG) with the lowest AIP in the section of the horizontal line (blue) [43].

It is these three hydrocarbons (RH **5**, **7,** and **10**) that were used in the present work to search for informative and analytically useful parameters of gas evolution–a previously unexplored and unaccounted-for factor that influenced the conversion of hydrocarbons. After the detection of the influence of hydrocarbons on the processes of gas evolution, the entire main set of RH **5**–**10** was used under the selected experimental conditions.

The additional components of the reaction mixture that were used in the present work are shown in Scheme 2. Salt $CuCl_2 \cdot 2H_2O$ (**12**) and complex $Cu(DMG\text{-}H)_2$ (**13**) are products of hydrolysis of the initial catalytic complex **1** [44]. The formation of oxygen-containing forms of Cu(II) copper compounds: salt oxide $CuO \cdot CuCl_2$ (**14**) and oxide CuO (**15**), could also be expected in this catalytic system.

2. Materials and Methods

Complexes **1** and **13** were synthesized according to the technique [44]. A 33% aqueous solution of hydrogen peroxide (H_2O_2) (Sigma-Aldrich, St. Louis, MI, USA) was used. The concentration of H_2O_2 was determined using a refractometer (IRF-22, Kazan, USSR) and calibration curve. Acetonitrile (CH_3CN) was qualified for HPLC (Sigma-Aldrich). Hydrocarbons and other catalysts purchased from different companies had a purity of at least 99% and were used without additional purification.

A sealed glass thermostated reactor (50 mL) was equipped with a jacket, a reverse refrigerator, and magnetic stirring. The return refrigerator was connected to a burette filled with water (100 mL). The catalyst was introduced last into the reaction mixture immediately after the addition of the oxidizer solution to acetonitrile. A fast method (~3 s) of introducing an oxidizer solution was used. The reaction temperature was 50 °C. The reaction time was not fixed. The experiments were stopped when the evolution of gas stopped.

The reagent ratio 33% H_2O_2 (mL)/CH_3CN (mL)/Catalyst **1** (mg)/Hydrocarbon (mL or g) was used: 0.34 or 0.5/5/10/0.1, except experiment 4E: 1.5/30/100/0.01.

Orca—an ab initio, DFT, and semiempirical SCF-MO package—version 3.0.1 was used for all DFT calculations in the PBE0/TZVPP level of theory [45,46].

The ChemCraft 1.7 program was used to create input files, and visualize and design the calculation results [47] (see sections below and Supplementary Materials Table S1).

3. Results and Discussion

3.1. Preliminary Experiments and Evolution of Molecular Hydrogen

The main purpose of the preliminary experiments without the addition of hydrocarbons was to find well-reproducible catalytic conditions, in which the maximum amount of molecular oxygen theoretically calculated by reaction 5 is evolved (the “normal“ mode of gas evolution).

As expected, the studied catalytic system was unstable. Different amounts of gas were evolved in different experiments. However, what was unexpected was that in some experiments, the measured volumes of gas evolved during the reaction significantly exceeded the maximum volumes of molecular oxygen theoretically calculated by reaction 5 (“abnormal“ mode of gas evolution).

To measure the volumes of gases that evolved during the reaction, the authors used a sealed system consisting of a reactor, a reverse refrigerator, and a 100 mL burette filled with water. The amount of 0.34 mL of a 33% aqueous solution of hydrogen peroxide was chosen so that the amount of molecular oxygen expected by reaction 5 would not exceed 100 mL, taking into account the leakage of 6.5 mL of water under its own weight in the absence of gas evolution. This volume (6.5 mL) was subtracted from the total measured volume of gas.

Despite all precautions, so much gas was evolved in the first experiment that all of the water flowed out of the burette. In the second experiment (Figure 2A-a), 74 mL of gas was evolved, and only in the third experiment (Figure 2A-b), an amount of gas (37 mL) was evolved, that was equal to the amount of molecular oxygen calculated by reaction 5 (37 mL)

and which was well reproduced in subsequent experiments of this series of experiments (Figure 2A-c,d).

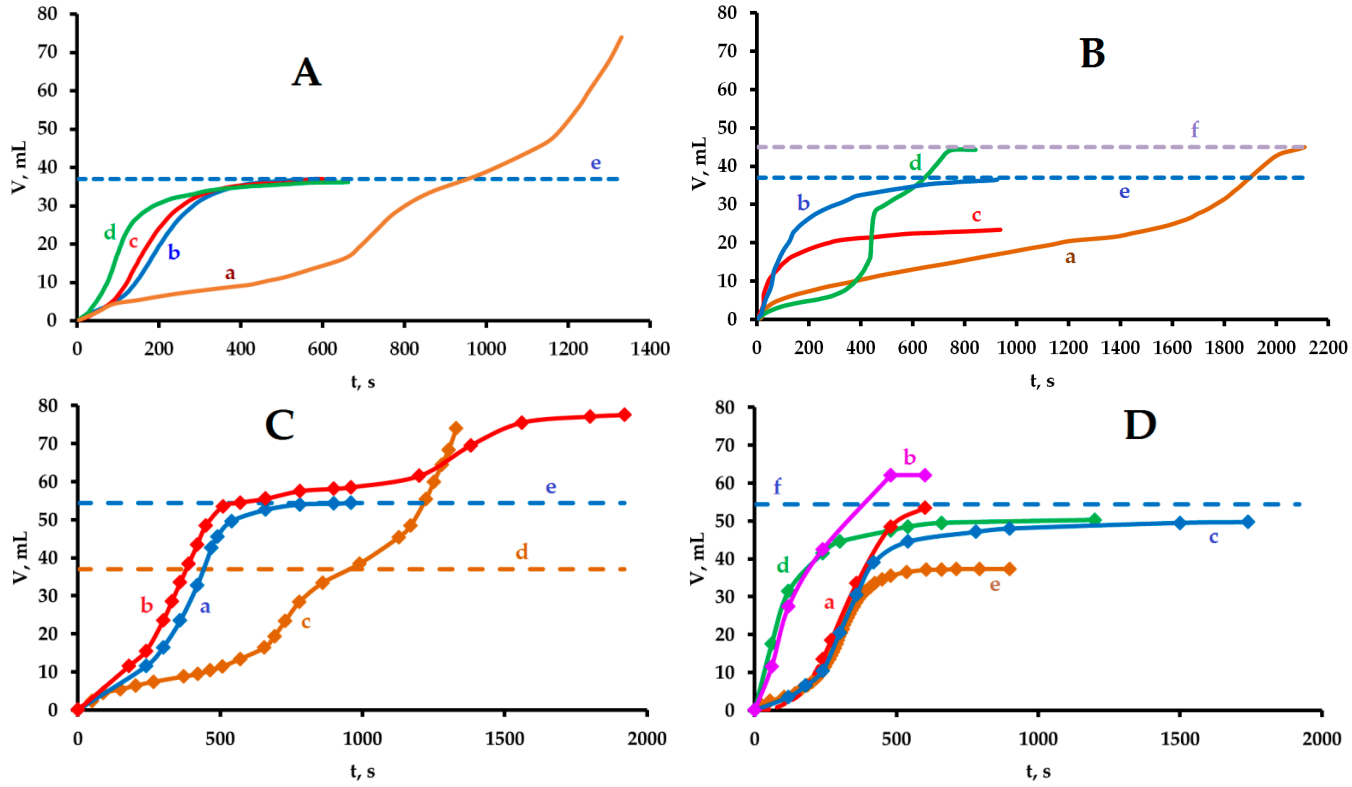

Figure 2. Kinetic curves of gas evolution. Reagent amounts: Cu(II) 40 μM in all cases, except (**B-d**) (12 μM); 33% H_2O_2 0.34 mL (3.3 mM) in (**A**,**B**,**C-c**) and 0.5 mL (4.9 mM) in the other cases; acetonitrile 5 mL in all cases, hydrocarbon RH **7** (0.1 mL, 830 μM) (**D**). Catalysts: Cu_2Cl_4·2DMG (**A-a**,**A-b**,**C**,**D**), $CuCl_2$·$2H_2O$ + DMG (1:1 mMs) (**A-c**), $CuCl_2$·$2H_2O$ (**A-d**), Cu(DMG-H)$_2$ (**B-a**), Cu(DMG-H)$_2$ + $CuCl_2$·$2H_2O$ + HCl (1:1:2 mMs) (**B-b**), CuO·$CuCl_2$ (Cu_2OCl_2) (**B-c**), CuO (**B-d**). The stirring speed is 400 revolutions per minute for all cases except (**D-a**,**D-b**,**D-d**) (correspondently 0, 200, 600 revolutions per minute). The reaction temperature was 50 °C. In experiment **C-b**, the reaction solution was kept for 10–15 min in the reactor before adding the catalyst. Equations of straight lines: V = 37 mL (**A-e**,**B-e**,**C-d**); V = 45 mL (**B-f**); V = 54.4 mL (**C-e**,**D-f**).

An additional amount of gas, namely molecular hydrogen, could be formed by two reactions: 2 and 4. During the transition from the second to the third experiment (Figure 2A-a,b), the amount of gas decreased by half. If one assumes that during the transition from the first to the second experiment, the amount of gas also decreased by half, then 148 mL of gas should have been formed in the first experiment. This amount of gas is exactly equal to the theoretical value of the maximum possible gas evolution by reaction 4 and, therefore, the expected ratio of the volumes of hydrogen and oxygen gases formed should have been equal to 1:1. This assumption requires experimental verification.

In the fourth and fifth experiments (Figure 2A-c,d), the same amount of gas–molecular oxygen was evolved as in the third experiment (Figure 2A-b). The same amounts of copper(II) ions were taken, but in different forms: complex **1**, salt **12**, and salt **12** + DMG (Figure 2A-b,c,d, respectively). Only the time of the onset of the active phase of gas evolution changed, and in experiments 2A-b,c this time had similar values and was significantly longer than in experiment 2A-d. This can be attributed to the fact that the evolution of molecular oxygen occurred after the destruction of complex **1**, resulting in the formation of a mixture of salt **12** + DMG.

In the next series of experiments, kinetic curves of gas evolution in model systems were determined (Figure 2B). A comparison of two pairs of curves 2B-a,b, and 2B-c,d shows that the catalytic activity of different forms of Cu(II) is not an additive quantity, but depends on the presence or absence of additional components.

The kinetic curves 2B-a (complex **13**) and 2B-b (complex **13** + salt **12** + 2HCl–hydrolysis products of complex **1**) differ greatly from each other and from the curve in Figure 2A-b (complex **1**). This indicates that the hydrolysis of complex **1** with the formation of complex **13** does not occur in the studied catalytic system. Visual observations, which will be described later, support this conclusion. The authors believe that in the 2B-b experiment, the complex **13** + 2HCl completely transformed into the salt **12** + 2DMG before the stage of active gas evolution.

The composition of the salt-oxide **14** includes two components: CuO and $CuCl_2$. The corresponding salt-oxide kinetic curve 2 B-c shows that less gas (O_2) is evolved (23.4 mL) than in experiment 2B-b (37 mL). The volume ratio 23.4:37 = 0.63 is exactly equal to the molecular weight ratio M($CuCl_2$): M(CuO·$CuCl_2$), which indicates that only the $CuCl_2$ salt is involved in the 2B-c experiment, and CuO oxide remains inactive.

The salt-oxide CuO·$CuCl_2$, light green in color, is partially soluble in acetonitrile. After the dissolution of the $CuCl_2$ salt included in its composition, the solution acquires a yellowish color and an insoluble precipitate of black color is formed–CuO oxide. It is this amount of CuO oxide that was used in the 2B-d experiment. In the absence of the $CuCl_2$ salt, CuO oxide became active, and almost twice as much gas (45 mL) evolved with its participation as in the 2B-c experiment (23.4 mL). At the same time, once again, as in experiment 2B-a, the evolution of a volume of gas was detected, which exceeded the maximum amount of molecular oxygen theoretically calculated by reaction 5 (37 mL).

In subsequent experiments (Figure 2C,D), the amount of the oxidizer solution was increased to 0.5 mL and a search was made for unaccounted factors that could affect different parameters of gas evolution. Theoretically calculated by reaction 5, the maximum volume of molecular oxygen evolved was equal to 54.4 mL.

Under standard conditions, which, among other things, included a verified sequence of operations with reagents, catalyst **1** was introduced into the reaction mixture last, after which the system was quickly sealed, and stirring of the reaction mixture was started and a gasometer was included. Under these conditions, the volume of the evolved gas was exactly equal to 54.4 mL (Figure 2 C-a).

It was found that during the reaction, the surface of the glass reactor was covered with a white coating, and a light green sediment was deposited on the bottom of the reactor. A description of the properties and the expected chemical composition of these two insoluble reaction products will be given in one of the following sections devoted to the description of the different forms of copper that have been used or obtained in the studied catalytic system.

When the reaction mixture was kept in the reactor for 10–15 min (with stirring) before the introduction of catalyst **1**, after the evolution of 54.4 mL of molecular oxygen gas, an additional amount of gas (23.1 mL) was evolved, and the total volume of gas reached 77.5 mL (Figure 2C-b). Since all hydrogen peroxide was consumed by the time the additional amount of gas was evolved, its source could only be water molecules by reaction 2, and the composition of the additional amount of gas had to be H_2:O_2 = 2:1.

This is the second striking example of an abnormally large amount of evolved gas. For ease of comparison, the same figure shows the first example (Figure 2C-c, the same as Figure 2A-a), in which a smaller amount of an oxidizer solution was used (0.34 mL), and the maximum amount of molecular oxygen by reaction 5 was 37 mL.

The next two possible unaccounted-for factors that were tested in experiments with the addition of hydrocarbon RH **7** were the speed of stirring and the uncontrolled "human" factor when the experiments were carried out by different hands, that is, by each author of this work separately (Figure 2D).

There are no regular changes in the parameters of the kinetic curves of gas evolution with an increase in the stirring speed in the series 0, 200, 400, and 600 revolutions per minute (Figure 2D-a–d). On the contrary, it was found that the time to reach the active phase of gas evolution was influenced by an uncontrolled "human" factor. Pairs of experiments 2D-a,c (0 and 400 revolutions per minute) and 2D-b,d (200 and 600 revolutions per minute) were made by different authors of this work, I.Y.S., and A.I.N., respectively. The two authors used different methods of preparing the reactor for the experiment, which was washed with acetonitrile in the first case and, consequently, with water and acetone in the second case.

In both cases, there was another uncontrolled factor that influenced the amount of gas that evolved (compare the curves inside the two pairs 2D-a,c, and 2D-b,d). By analogy with previous experiments, this unaccounted factor could be the sequence in a series of experiments. Therefore, at a standard stirring speed of 400 revolutions per minute, six experiments were carried out in a row without measuring the volume of gas evolved, and for the seventh time, a 2D-e kinetic curve was obtained, in which a well-reproducible and smallest amount of gas (37.3 mL) was evolved. It was these verified conditions that were used in the next series of experiments with other hydrocarbons as uniformly and consistently as possible one after another (see next section).

The 2D-a experiment without stirring allowed for making valuable visual observations. At the initial moment of time immediately after the addition of complex **1**, the following was observed. The walls of the glass reactor were covered with a white coating. At the bottom of the reactor, blue-green crystals of complex **1** lay in a "slide". The reaction solution, consisting of a solution of an oxidizer and acetonitrile, was transparent and colorless. No gas evolution occurred during the first 10 ± 5 s. Further, the reaction solution began to turn yellow and after reaching a certain intensity of yellow color, which was then maintained approximately constant, there was an intense evolution of gas from the surface of the white coating. As the gas evolved, the crystals of complex **1** decreased in size until their complete disappearance. No gas was formed on the surface of the crystals of complex **1**. After some noticeable decrease in the intensity of the yellow color of the reaction solution, the gas evolution stopped. Thus, in the 2D-a experiment, molecular oxygen was formed only on the surface of the white coating. In total, 53.5 mL of gas was evolved in this experiment (Figure 2D-a), which is close to the theoretical value of 54.4 mL of molecular oxygen formation by reaction 5.

Note that the yellow color of the reaction solution of the 2D-a experiment means the formation of a new chemical form of copper soluble in acetonitrile from complex **1**, since, without the addition of an oxidizer solution, complex **1** retains its blue-green color in freshly prepared acetonitrile solutions.

3.2. Experiments in the Presence of Hydrocarbons and the Evolution of Molecular Oxygen

In experiments with the presence of hydrocarbons (see Scheme 1), the conditions of the 2D-e experiment were used. Upon quantitative decomposition of 0.5 mL of an aqueous solution of the oxidizer 33% H_2O_2 by reaction 5, 54.4 mL of molecular oxygen is formed (Figure 2C-a). When hydrocarbons are added to the reaction mixture, the amount of molecular oxygen formed decreases. Other parameters of kinetic curves also change.

For the three test hydrocarbons RH **5**, **7**, and **10**, the same type of kinetic curves of gas evolution (O_2) were obtained (Figure 3A,B). Three parameters of the gas evolution curves: the maximum volume of the evolved gas (Figure 3A), the time to reach the middle of the interval of the active phase of gas evolution, and the rate of gas evolution in these areas, that is, the slope of the straight lines with the proportionality coefficient "a", (Figure 3B), change in a consistent and regular manner (Figure 3C,D).

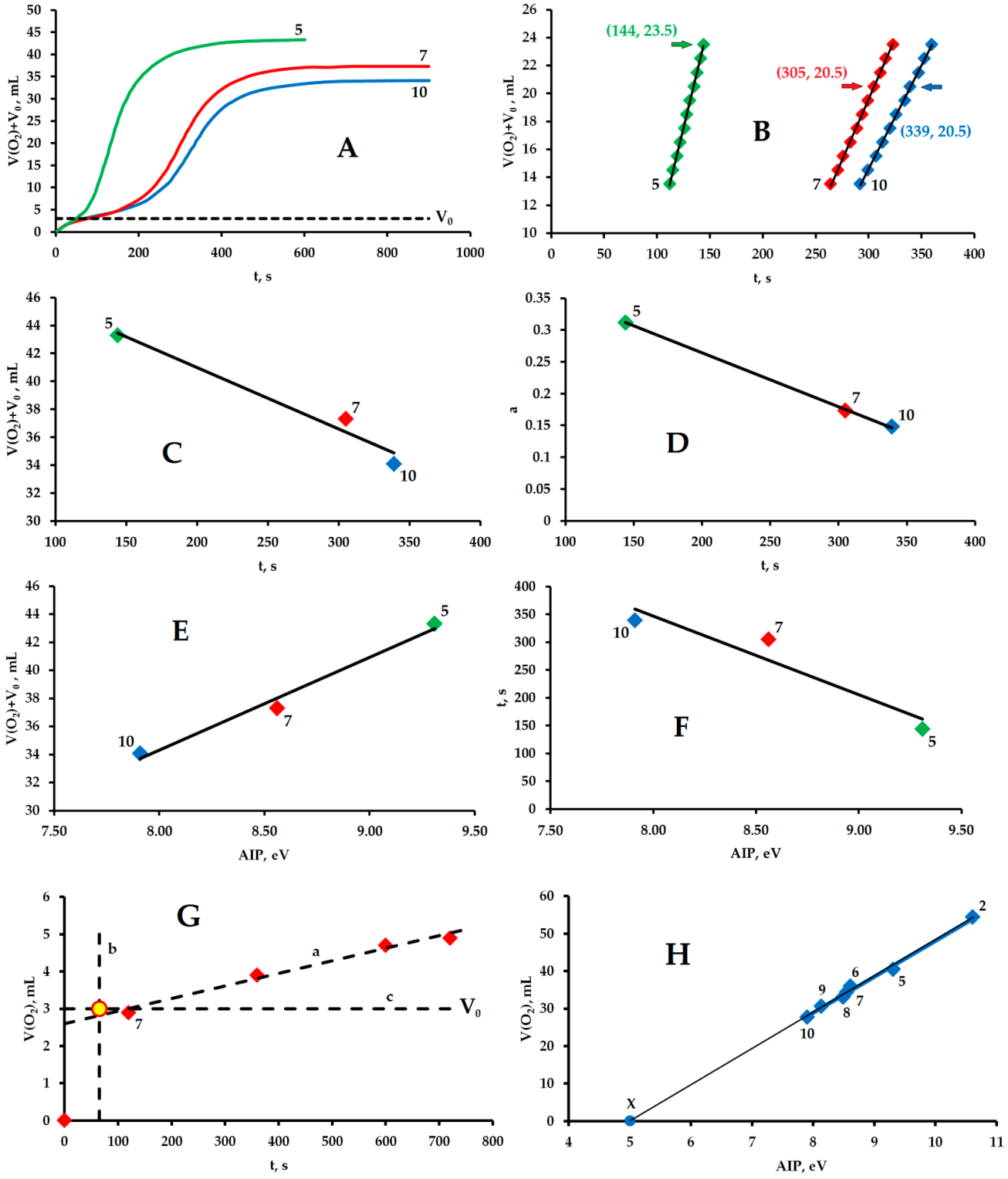

Figure 3. Kinetic curves (**A**,**B**,**G**) and correlations of their parameters with each other and with the AIP of hydrocarbons RH and H_2O_2 (**C**–**F**,**H**). Equations of straight lines **y = ax + b**: (**A**): V_0 = 3 mL; (**B**): $V(O_2) + V_0 = 0.312t - 21.522$, $R^2 = 0.9984$ (RH **5**), $V(O_2) + V_0 = 0.1733t - 32.406$, $R^2 = 0.9989$ (RH **7**), $V(O_2) + V_0 = 0.1481t - 29.85$, $R^2 = 0.9993$ (RH **10**); (**C**): $V(O_2) + V_0 = -0.0441t + 49.808$, $R^2 = 0.9659$; (**D**): **a** = –0.0008t + 0.4336, $R^2 = 0.9996$; (**E**): $V(O_2) + V_0 = 6.6078AIP - 18.55$, $R^2 = 0.9825$; (**F**): t = –141.21AIP + 1476.1, $R^2 = 0.901$; (**G**): (a) $V(O_2) = 0.0034t + 2.5746$, $R^2 = 0.9841$, (b) t = 65 s, (c) $V_0 = V(O_2) = 3$ mL; (**H**): $V(O_2) = 9.624AIP - 48.117$, $R^2 = 0.9939$.

These three parameters are linearly related to each other, that is, they are not independent of each other. Therefore, it is adequate to monitor only one parameter, not three.

Since the kinetic curves were taken manually, it was most convenient to determine a well-reproducible maximum volume of the evolved gas in a series with hydrocarbons without laborious recording and processing of detailed kinetic curves.

The volume V of the evolved gas and the time t to reach the middle of the interval of the active phase of gas evolution linearly depend on the AIP of the three test hydrocarbons (Figures 3E and 3F, respectively).

In contrast to the dependence of D(O) on AIP (Figure 1B), the dependence of V on t has no break at the point RH **7**, and on the interval of points, RH **7** and RH **10**, has a directly proportional, not inversely proportional, slope of a straight line. This, in the authors' opinion, indicates that the oxidation of hydrocarbons and the evolution of molecular oxygen occurs on different catalytic forms of copper. The oxidation of hydrocarbons occurs with the participation of the initial catalytic complex **1** before its destruction, after which a new form of copper is formed, which catalyzes the process of molecular oxygen evolution.

The inversely proportional dependence of t on AIP (Figure 3F) shows that with a decrease in AIP RH, the time t increases until the beginning of the active phase of gas evolution. This means that with a decrease in AIP RH, the lifetime of the initial complex **1** increases, respectively, the time period during which hydrocarbons with AIP having equal AIP RH **7** or lower values are oxidized increases.

In addition to the active phase of the molecular oxygen evolution in the studied catalytic system, there is an additional source, which acts at the initial stage for times less than 100 s and gives an additional V_0 = 3 mL of gas (Figure 3A). Taking into account the fact that the stirring speed does not affect the gas formation processes and it is possible to use the stirring speed of 0 instead of 400 revolutions per minute (Figure 2D), the authors conducted such an experiment without adding a catalytic complex **1** (Figure 3G) in order to use visual observations to determine the source of an additional amount of molecular oxygen in the initial section of kinetic curves, shown in Figure 3A.

In the 3G experiment, there was only a white coating on the walls of the reactor as a catalyst. The solution quickly turned yellow. Gas began to be evolved from the surface of the white coating. Several registered points of the kinetic curve are located along the 3G-a straight line. The solution became colorless again. The evolution of gas stopped.

The point at the intersection of the 3G-b and 3G-c lines is located in the vicinity of the 3G-a line. The value t = 65 s is the average value of the intersection points of three kinetic curves 3A-5,7,10 with a straight line V_0 = 3 mL. Thus, the value V_0 = 3 mL that has been taken as an estimate has an accuracy of at least 0.4 mL at the time interval t = 0–235 s from the start of the reaction (Figure 3G).

The values of $V(O_2) = (V(O_2) + V_0) - V_0$ used in Figure 3H are those quantities of $V(O_2)$ gas that were evolved only with the participation of copper ions injected into the reaction solution with a new portion of complex **1**. The AIP values of **2** and RH **5**–**10** were taken from [43]. All experimental points are located along a straight line, the parameters of which are highlighted in blue in the caption of Figure 3H. According to this line, the gas evolution will stop ($V(O_2)$ = 0) if a substance X with AIP = 5.0 eV is added to it.

3.3. Some Additional Experiments and the Oscillatory Mode of Gas Evolution

In this paper, the authors have tried to preserve all the ratios of the main reagents and solvent that were previously used in experiments on the oxidation of hydrocarbons [43]. To verify that the catalytic conditions have not changed significantly, the composition of the oxidation products of RH **7** in experiment 3A-7 was determined using chromatography-mass spectrometry (for details of the analysis, see [43]).

In accordance with the new systematization method, the total amounts of products that included one and two oxygen atoms were calculated to determine the oxidation depth D (%) of RH **7**. Mono- and di-oxygenated products of RH **7** oxidation are designated by the symbols: 1O and 2O, respectively.

The oxidation of RH **7** (conversion C = 29%) produced the products 1O: alcohols **7a** (10%), **7b** (4%) and **7c** (14%), aldehyde **7d** (41%); 2O: diols **7e** (10%), alcohol-aldehyde **7f** (4%), acid **7g** (7%) and diketone **7h** (10%) (Scheme 3). The sum of the products 1O and 2O, respectively, is 69 and 31%. The oxidation depth D(O) = 131%, SOP = 203%, TON = 24, where the sum of products SOP = 1·1O + 2·2O, the formula for calculating TON (turnover number) is given in [43]. The previously obtained result of RH **7** oxidation was as follows: C = 20%, D(O) = 121%, SOP = 167%, and TON = 7 [43].

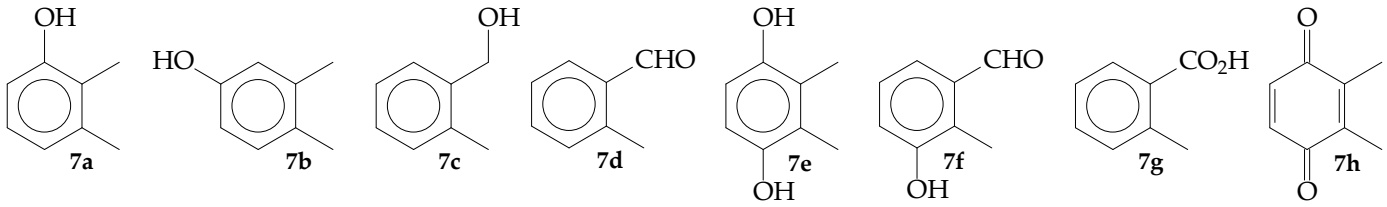

Scheme 3. Products of oxidized hydrocarbon RH **7**.

In this study, the initial concentration of RH **7** was increased by 10 times compared to the study [43]. The sets of characteristics of the mixture of RH **7** oxidation products obtained in the two studies have similar values, which indicates that the catalytic conditions have not changed significantly.

A new series of experiments with RH **7** was carried out (dependencies 4A-a and 4B-a in Figure 4A,B), in which the amount of evolved gas V and the time t to reach its maximum value were determined, respectively, depending on the mass of complex **1** (A.I.N.) introduced into the reaction mixture. For comparison, those figures show data 4A-b and 4B-b, respectively, of experiments 3G (m = 0 mg) and 3A-7 (m = 10 mg) (I.Y.S.). In Figure 4A,B, the experimentally obtained data are displayed in squares, and the estimated data are displayed in circles.

As in previous cases, the method of processing white coating in preparing the reactor for the upcoming experiment had a strong impact on the result. With method "a" (A.I.N.), there is a dependence on m, and with method "b" (I.Y.S.), there is no such dependence (Figure 4B). The values V = 9.8 mL (point 4A-a) and t = 1440 s (point 4B-a) expected at m = 0 mg are exactly twice as large as the experimental values V = 4.9 mL (point 4A-b) and t = 720 s (point 4B-b).

The authors' observation shows that the method of pretreatment of the reactor and the moment of its sealing could be uncontrolled sources of a spread from 0 to 10 mL in the measured volumes of the evolved gas, which at V < 54.4 mL could be observed in the first experiments (Figure 2D).

Figure 4B also shows another estimated point with m = 30 mg and t = 0 s, which corresponds to an instantaneous (explosive?) allocation of the maximum volume of gas. This type of effect has sometimes been observed in the oxidation of hydrocarbons. In some experiments, there was such a rapid and intense evolution of gas that the reaction solution was ejected through the return refrigerator into the atmosphere. It was not exactly understood what this action related to.

An unexpected result was obtained with RH **11** (Scheme 2) (Figure 4C). It was intended to measure only the final volume V of the emitting gas. For this reason, only a few points are shown in Figure 4C and the dotted line shows the simplest possible form of the kinetic curve, which has not been determined experimentally.

After reaching the volume of gas V = 47 mL, the catalytic system unexpectedly switched to a well-reproducible and stable oscillatory mode of gas evolution: approximately 0.1 mL in one oscillation with an interval of 2–3 s. In this mode, an additional 12 mL of gas was evolved, and its final volume reached the value V = 59 mL, which slightly exceeded the value $V(O_2)$ = 54.4 mL expected for reaction 5.

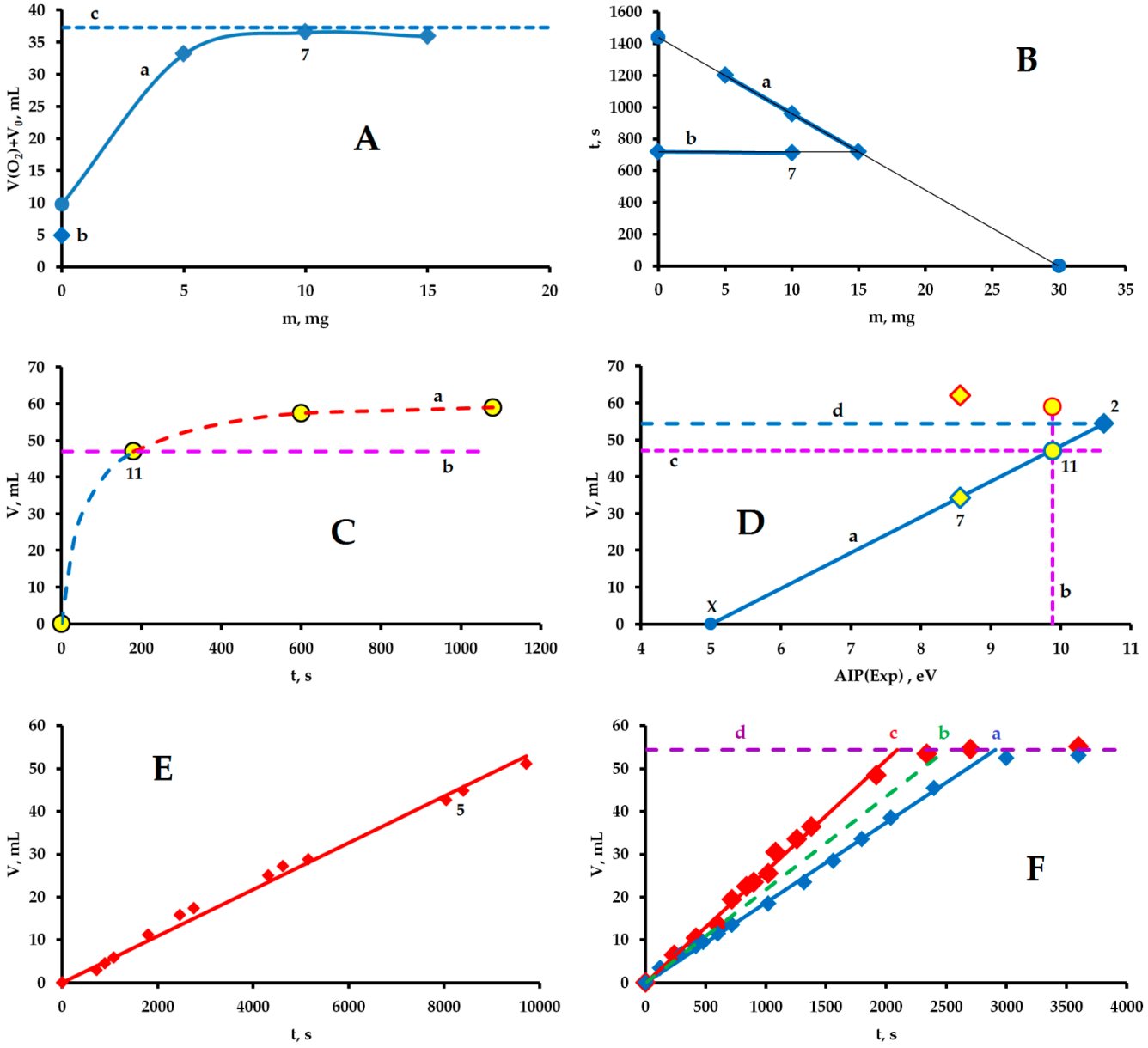

Figure 4. Additional experiments with RH **7** (**A**,**B**), **11** (**C**), **7** and **11** (**D**), **5** (**E**), 0.1 mL RH **7** + 4.6 mg DMG (**F**). The stirring speed is 400 revolutions per minute for all cases except (**E**,**F-a**,**F-b**,**F-c**) (correspondently 0, 200, 400, 600 revolutions per minute). The reaction temperature was 50 °C for all cases except (**E**) (0 °C). An oscillatory mode of gas evolution is selected by the red collar in experiments **C** and **E**. Equations of straight lines **y = ax + b**: (**A**): V_0 = 37.3 mL; (**B**): (a) t = −48m + 1440, R^2 = 1, (b) t = 720 s; (**C**): (b) V = 47 mL; (**D**): (a) V = 9.624AIP − 48.117, R^2 = 0.9939, (b) AIP = 9,88 eV (RH **11**), (c) V = 47 mL, (d) V = 54,4 mL; (**E**): V = 0.0054t, R^2 = 0.9924; (**F**): (a) V = 0.0187t, R^2 = 0.9974, (b) V = 0.0224t (average (a) and (c)), (c) V = 0.026t, R^2 = 0.9625, (d) V = 54,4 mL.

For RH **11**, the point with AIP = 9.88 eV and V = 47 mL exactly lay on the 4D-a straight line (the same as the straight line in Figure 3H). For H_2O_2 (**2**), the point with AIP = 10.62 eV and V = 54.4 mL also exactly lay on the 4D-a straight line. In the 2C-b experiment (without the addition of hydrocarbons), after reaching the value V = 54.4 mL, the catalytic system also switched to the mode of abnormal gas evolution.

Thus, line 4D-a is the boundary (lines 4D-b,c for RH **11**), and upon reaching it, becomes possible for the system to transition into an anomalous oscillatory mode of gas evolution.

In the case of RH **7** with AIP = 9.56 eV and V = 34.3 mL, after reaching this limit, the system also switched to an anomalous oscillatory mode of gas evolution (2D-b experiment, the final value of V = 62.1 mL), which the authors did not pay much attention to at first.

Since in all these three cases (**2**, RH **11,** and **7**), an abnormally large amount of gas is evolved (more than V = 54.4 mL (line 4D-d)), the authors believe that after reaching the boundary, a line 4D-a, gas is evolved abnormally in the oscillatory mode consisting of a mixture of molecular hydrogen and molecular oxygen, the ratio of which is not known.

In experiment 4E with RH **5**, at T = 0 °C, without stirring and white coating on the walls of the reaction flask, with the increased quantities of the main components of the reaction mixture (H_2O_2 by 3 times), an oscillatory mode of gas evolution was established from the very beginning: approximately 0.2 mL in one oscillation with an interval of 25 ± 5 s. As can be seen from Figure 4E, all experimental points (t,V) were located along a straight line, and the evolution of gas occurred in direct proportion to the reaction time.

The peculiarity of this reaction was that all RH **5** concentrated on the top surface of the acetonitrile solution, in which, is not soluble at that temperature. Therefore, one can assume that this experiment was carried out in the absence of RH **5**. The second unusual fact was that the solution had the blue-green color of the original complex **1**.

The evolution of gas was slow: 51.2 mL of gas evolved in 9720 s from 163.2 mL expected by reaction 5. Therefore, the reaction, which was at its initial stage, was stopped. The composition of the gas remained unknown.

The initial concentration of hydrocarbons was not varied, since its increase by 10 times did not significantly affect the composition of the oxidation products, but led to a noticeable and expected decrease in the conversion of hydrocarbons [43].

Instead of this type of experiment, the authors conducted a new type of experiment (Figure 4F): under the conditions of 2D-b,d experiments, 4.6 mg of DMG was added to 0.1 mL of RH **7**. The gas evolution became linear up to the maximum value V = 54.4 mL.

If, in the 2D-b,d experiments, the linear sections of the rapid gas evolution stage are extrapolated to the maximum value, it can be seen that the addition of a significantly smaller amount of DMG than RH **7** led not only to an increase in the length of the linear gas evolution section but also increased the time to reach the maximum gas volume by more than an order of magnitude.

As a result, the effect of the stirring speed of the reaction mixture on the processes of gas formation became noticeable. Figure 4F shows three straight lines: two experimental and one averaged, which correspond to stirring speeds of 200, 400, and 600 revolutions per minute. Based on the fact that the maximum volume of gas is 54.4 mL, it can be concluded that only molecular oxygen evolved under these conditions.

3.4. Catalytic Forms of Copper and Identification of Component X

Under the catalytic conditions used, the authors observed the presence of four forms of copper compounds: soluble in acetonitrile blue-green starting complex **1** and the yellow compound (**16**) formed from it, and insoluble in the acetonitrile white coating (**17**) and light green precipitate (**18**). The fifth form of copper was also present in the system–X (**19**), which could not be seen visually, but whose presence followed from the dependence of AIP and V (extrapolation of the line in Figure 3H and the same line 4D-a before the intersection with the AIP axis).

Physicochemical methods established that in the crystalline state, complex **1** (Cu_2Cl_4·2DMG, Scheme 1) had a dimeric structure [44,48–50]. The spatial structure and geometric parameters of complex **1** were determined by X-ray diffraction analysis [44], systematically discussed in the review [51] and in theoretical papers [52,53]. Since the color of the crystals and the freshly prepared acetonitrile solution were the same, it can be concluded that complex **1** retains its dimeric structure in the acetonitrile solution as well.

Holding acetonitrile solutions of complex **1** without and with the addition of 0 and 33% aqueous solutions of hydrogen peroxide, taken in standard quantities in this work, at 25 and 50 °C, leads to a change in the blue-green color of the solution to yellow.

According to the authors' opinion and the literature data, the yellow color of the acetonitrile solution will originate from the $Cu_2Cl_4 \cdot 2CH_3CN$ (**16**) complex, which is formed as a result of the ligand exchange reaction 15. The chemical composition and dimeric structure of the yellow complex **16**, which was observed in acetonitrile, was previously established by physicochemical methods [54–56]. Three complexes of the general composition $(CuCl_2)_n \cdot 2CH_3CN$ isolated in crystalline form and of the same spatial structure had different colors: blue, yellow, and red at n = 1, 2, and 3, respectively [54].

$$Cu_2Cl_4 \cdot 2DMG + 2CH_3CN \rightarrow Cu_2Cl_4 \cdot 2CH_3CN\ (\mathbf{16}) + 2DMG \quad (15)$$

In the authors' opinion, a white coating forms copper monochloride CuCl (**17**) on the walls of the glass reactor–a product of redox reaction 16. Salt CuCl is insoluble in water, acetonitrile, acetone, and other organic solvents. Its white coating was dissolved only in a partially spent chromic and sulphuric acids mixture (brown).

$$Cu_2Cl_4 \cdot 2CH_3CN + H_2O_2 \rightarrow 2CuCl\ (\mathbf{17}) + 2HCl + O_2 + 2CH_3CN \quad (16)$$

If one assumes that reactions 15 and 16 occur quantitatively, then the molar ratios of the reagents are equal: **1**:**16** =1:1 and **16**:**2** = 1:243, respectively. The catalytic amount of complex **16** formed in a large deficiency (by more than two orders of magnitude) is sufficient to produce only 0.22 of the 54.4 mL of O_2 expected by reaction 5. Therefore, ideas about the cyclic method of O_2 formation, which are based on reactions 7 and 8, are traditionally attracted.

The light green complex **18** was similar in appearance to salt **14**, but its properties were very different from it. Unlike salt **14**, complex **18** was not active in the O_2 formation reaction and did not dissolve in acetonitrile, giving a black precipitate–CuO oxide.

To determine the ratio of copper ions, which are included in salt **17** and compound **18**, and the possible chemical composition of compound **18**, a 2C-a experiment was conducted with 20 times increased amounts of reagents and solvent, and a reaction time of 1800 s.

According to the elemental analysis, the isolated and dried light green precipitate **18** contained 58.69% copper atoms, a small number of oxygen atoms (~2–5%), and did not contain chlorine atoms, which corresponds to the compound $(CuCH_3CN)_6 \cdot 1H_2O$ (59.06% Cu atoms), $(Cu_3H \cdot 3CH_3CN)_2 \cdot 1H_2O$ (58.87% of Cu atoms), $Cu_4O \cdot 4CH_3CN$ (58.52% of Cu atoms), or some other compound with a similar chemical composition. The copper atoms of the initial complex **1** entered compounds **17** and **18** in a ratio of 1 to 2, respectively.

To designate compound **18** participating in reaction 17, the formula $CuCH_3CN$ (60.60% of copper atoms) was introduced, which is a simplification (compound **~18**), and not one of the possibilities contain the maximally reduced atomic form of copper in its composition, which is convenient for carrying out evaluation calculations. If the entire amount of complex **16** is involved in reaction 17, then 0.44 mL of O_2 gas (maximum value) will be evolved from the 54.4 mL expected by reaction (5).

$$Cu_2Cl_4 \cdot 2CH_3CN + 2H_2O_2 \rightarrow 2CuCH_3CN\ (\mathbf{\sim 18}) + 4HCl + 2O_2 \quad (17)$$

The glass reactor, with a volume of 50 cm^3, had a diameter of d = 3 cm and a height of H = 7 cm. The reaction volume had a height h = 0.8 cm and was limited by a glass surface $S_r = 1.45 \cdot 10^{-3}$ m^2.

At 50 °C, the CuCl salt had a cubic structure of zinc blende, in which Cu^+ cations were located in the center of a tetrahedron formed by Cl^- anions [57–62]. One unit cell consists of four CuCl molecules. Based on the value $a_0 = 5.416 \cdot 10^{-10}$ m of the lattice parameter, the distance between the Cu and Cl atoms was $2.345 \cdot 10^{-10}$ m, and the S_e surface of one square face (Cu, Cu, Cu, Cu [59,62]) was $29.33 \cdot 10^{-20}$ m^2.

Consequently, one monolayer of CuCl, which covers the entire glass surface of the reaction volume, contains $S_r/S_e = 4.94 \cdot 10^{15}$ square elemental cells and twice as many ($9.88 \cdot 10^{15} \approx 10^{16}$) CuCl molecules.

If the entire amount of $CuCl_2$ ($4 \cdot 10^{-5}$ mol) contained in $2 \cdot 10^{-5}$ mol of complex **1** passes into CuCl, then such molecules would form $2.4 \cdot 10^{19}$, which means planting 2400 layers of CuCl in one standard experiment. Since only one-third of all copper atoms of complex **1** pass into CuCl salt and the thickness of the CuCl monolayer was $0.5a_0 = 2.7 \cdot 10^{-10}$ m, 800 CuCl layers with a total thickness of 216 nm are planted in one standard experiment.

The value of AIP(X) = 5.0 eV, which is too small for neutral molecules and radicals, indicates the participation in the process of single ionization of radical anions (RA), which were formed from molecules (Mol) with a large (5.0 eV) adiabatic electron affinity (AEA) since AEA(Mol) = AIP(RA). Such molecules are copper chlorides with the general formula Cu_nCl_m, where n = 1, 2, m = 2–5, for which experimental and calculated theoretical methods have obtained AEA values in the range from 4.3 to 5.5 eV [63].

Next, the procedure for searching using density functional theory (DFT) calculations of the structure of the Cu_nCl_m molecule, for which AEA = 5.0 eV, will be presented (Figures 5 and 6, Table 1).

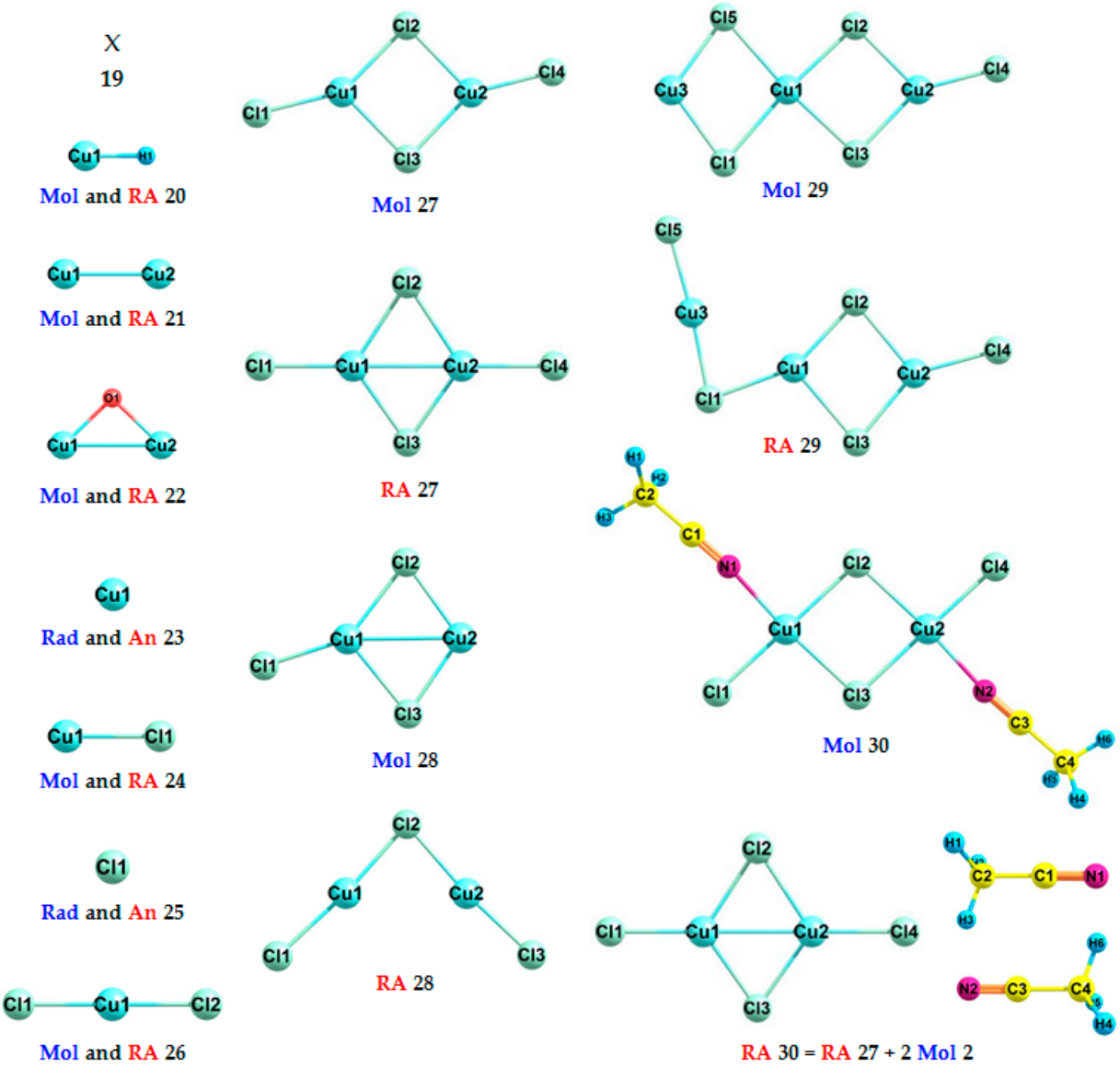

Figure 5. The DFT calculated molecules (**Mol**), radicals (**Rad**), radical anions (**RA**), and anions (**An**).

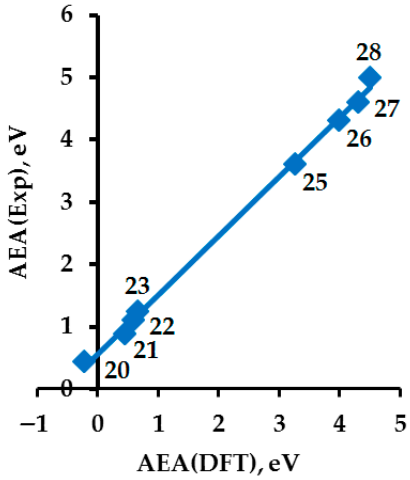

Figure 6. Correlations between DFT calculated and experimental values of AEA: AEA(Exp) = 0.9516AEA(DFT) + 0.5533, R^2 = 0.9978.

Table 1. Experimental and DFT calculated adiabatic electron affinities (AEA, eV) and DFT calculated energies (E, E_h) of molecules (**Mol**) or radicals and radical anions (**RA**) or anions of **19**–**30** *.

Formula	No.	Exp.	DFT	A·DFT+B	E(Mol or Radical)	E(RA or Anion)
X	**19**	**5.00**	**4.66**	**5.00**	-	-
CuH	**20**	0.444 ± 0.006 [64]	−0.21	0.34	−1640.833185884078	−1640.825562232613
Cu_2	**21**	0.88 ± 0.02 [65]	0.45	0.97	−3280.540332075323	−3280.557003438048
Cu_2O	**22**	1.10 ± 0.03 [66]	0.6	1.12	−3355.687224138422	−3355.709345013066
Cu	**23**	1.235 ± 0.005 [67]	0.67	1.18	−1640.236451203338	−1640.261078219124
CuCl	**24**	-	0.91	1.41	−2100.368056439018	−2100.401477462000
Cl	**25**	3.6127 ± 0.0001 [68]	3.27	3.67	−459.996618462930	−460.116771209037
$CuCl_2$	**26**	4.3 ± 0.1 [63]	4.00	4.37	−2560.458515677480	−2560.605611152270
Cu_2Cl_4	**27**	4.6 ± 0.1 [63]	4.32	4.67	−5120.975980754558	−5121.134650902112
Cu_2Cl_3	**28**	5.0 ± 0.2 [63]	4.36	4.70	−4660.897876026251	−4661.057919072903
Cu_3Cl_5	**29**	-	4.68	5.02	−7221.407385765084	−7221.579242854321
Cu_2Cl_4·2AN	**30**	-	3.07	3.48	−5386.306768478984	−5386.419549320808

* DFT calculated AEA = (E(Mol or Radical) − E(RA or Anion))·27.2113834. The coefficients A = 0.9516 and B = 0.5533 were used. The estimated value AEA(X) = (5.00 − B)/A = **4.66** eV was used as an indicator for DFT calculations. Experimental AEA(Cl) = 29138.3 ± 0.5 cm^{-1} [68], 1 eV = 8065.54477 cm^{-1}. Based on the results of DFT calculations: X (**19**) = $Cu_3Cl_5^{\bullet-}$ (**RA 29**).

The need for such a search was also caused by the fact that the structure of the Cu_2Cl_3 molecule with an experimental value of AEA = 5.0 eV [63] was not suitable for the purpose of this study due to mechanistic considerations and due to the fact that this value, as the authors have established, is overestimated.

In earlier studies, only experimental values of AIP(RH) were used (see Figures 3E,F,H and 4G). Therefore, the AEA values of Cu_nCl_m molecules and related structures calculated by the DFT method were converted using the constructed correlation into experimental AEA values (Figures 5 and 6, Table 1).

This approach showed that the adjusted experimental value of AEA(Cu_2Cl_3) = 4.7 eV, which is significantly less than the desired value of 5.0 eV (Table 1). The structure of the Cu_3Cl_5 molecule, for which the evaluation procedure used by them gave an experimental value of 5.02 eV (Table 1), can be considered as the addition of a dimeric Cu_2Cl_4 molecule

from the acetonitrile-soluble complex **30** to a monomeric CuCl (**24**) molecule located on the surface of a white coating.

To emphasize that Table 1 uses data for single molecules in the gas phase, the authors have introduced new numbers for the some previously designated compounds. Instead of CuCl (**17**) salt, which is understood as a crystalline compound–a white coating on the glass surface of the reactor, CuCl (**24**) was introduced to denote the monomeric form located on the surface of the white coating. Instead of $CuCl_2 \cdot 2H_2O$ (**12**), $CuCl_2$ (**26**) was introduced, which does not contain water molecules. Instead of the $Cu_2Cl_4 \cdot 2CH_3CN$ (**16**) complex dissolved in the acetonitrile solution, the designation $Cu_2Cl_4 \cdot 2AN$ (**30**) was introduced for the same complex, but located in the gas phase, for which, unlike **16**, there is no need to take into account the influence of the composition of the liquid solution.

When one electron is attached to complex **30**, two acetonitrile (AN) molecules detach from RA $Cu_2Cl_4^{\bullet -}$ (Figure 5). Molecule **30** has a significantly lower (3.48 eV) AEA value compared to molecule **27** (4.67 eV), which does not include two acetonitrile molecules.

Thus, based on DFT calculations, the X compound in Figure 3H (and on the 4D-a line) has the chemical composition and structure of RA $Cu_3Cl_5^{\bullet -}$ (**29**).

3.5. Initiation of the Reaction of Molecular Oxygen Evolution by the SET Mechanism

At the ends of the straight line in Figure 3H (the same as the straight line 4D-a), there are two points that indicate the participation in the formation of molecular oxygen of the processes 18 and 19 of single ionization of the molecule H_2O_2 (**2**) and RA $Cu_3Cl_5^{\bullet -}$ (X = RA **29**).

$$Cu_3Cl_5 + H_2O_2 \rightarrow Cu_3Cl_5^{\bullet -} + H_2O_2^{\bullet +} \quad (18)$$

$$Y^{(\bullet)+} + Cu_3Cl_5^{\bullet -} \rightarrow Y^{(*)} + Cu_3Cl_5 \quad (19)$$

Reaction 18 is the first stage of the SET mechanism of activation of the H_2O_2 molecule, which was previously summarized as reaction 11. According to the authors' data, reaction 18 is activated only when there are conditions for the formation of the Cu_3Cl_5 molecule with the highest (5.0 eV) AIP value in this system. By the time molecular oxygen evolved, other forms of copper (**16** and **17**) with lower AIP values were present in the catalytic system, which did not allow them to trigger the reaction 18.

In the gas phase, reaction 18 is very endothermic, will not spontaneously proceed, and requires an external energy supply equal to $AIP(H_2O_2) - AEA(Cu_3Cl_5) = 10.62 - 5.0 = 5.62$ eV.

Perhaps for this energy reason, too, during the transition from gaseous to condensed media, instead of reaction 11, it is customary to give reaction 7, which makes it possible not to focus attention on how exactly the first stage of the SET mechanism is implemented.

The authors believe that during the transition from a gaseous to a condensed medium, several changes occur that favor the course of the reaction 18.

So, for example, the electron paramagnetic resonance (EPR) method shows that in liquid acetone, acetonitrile, and other solvents, a single electron transfer (SET) reaction occurs from N, N-dimethylaniline (DMA), AIP(DMA) = 7.10 ± 0.02 eV [69], to anhydrous $CuCl_2$ (**26**), $AEA(CuCl_2) = 4.37$ eV (Table 1), salt precipitates, which includes the radical cation (RC) $DMA^{+\bullet}$ [70].

Despite the fact that $AIP(DMA) - AEA(CuCl_2) = 2.73$ eV, in an ampoule filled with nitrogen, the EPR method observed the transformation of a quartet of lines of the molecule **26** into a multiplet belonging to RC $DMA^{\bullet +}$, that is, the reaction 20 was observed [67].

$$CuCl_2 + DMA \rightarrow CuCl_2^{\bullet -} + DMA^{\bullet +} \quad (20)$$

When using $CuCl_2$ molecules as the initiator of reactions, ideas about the implementation of the SET mechanism by reaction type 20 are widely used in describing chemical transformations of other amines [71–78].

Compared with the $CuCl_2$ molecule, the Cu_3Cl_5 molecule has an AEA greater by 5.0 − 4.37 = 0.63 eV. Consequently, it can be expected that Cu_3Cl_5 molecules in acetonitrile will be able to oxidize compounds with an AIP of at least 7.10 + 0.63 = 7.73 eV.

For water molecules, the first vertical and adiabatic potentials (VIP and AIP, respectively) within the error limits have the same values. It was experimentally determined that during the transition from a gas to a liquid medium, due to the formation of a hydrogen bond system, the value of AIP(H_2O) (≈VIP(H_2O)) decreased by 1.45 eV from 12.60 to 11.15 ± 0.05 eV and at the same time, the threshold of photoionization of liquid water was found to be 9.9 eV [79], which was close to another reported value for liquid water AIP(H_2O) = 10.12 ± 0.15 eV [80].

Thus, it can be assumed that with the transition from a gas to a liquid medium, the AIP(H_2O) value decreases by 12.6 − 9.9 = 2.7 eV.

For the gas phase in a series of clusters $(H_2O)_n$, where n = 1–8, close, but not equal to 9.9 eV, experimental data were obtained on a decrease in AIP by 1.7 eV with an increase in n from 1 to 8: AIP(H_2O) = 12.62 eV and AIP($(H_2O)_8$) = 10.92 eV [81].

A similar situation is observed with H_2O_2 molecules during the transition from the gas phase (experimental values VIP(H_2O_2) = 11.65 ± 0.57 eV [82,83], AIP(H_2O_2) = 10.62 eV [84], 10.685 ± 0.005 eV [85]) to a solution of H_2O_2 in water (VIP(H_2O_2) = 9.95 ± 0.60 eV [82,83]), that is, the VIP value decreases by 11.65 − 9.95 = 1.7 eV.

As can be seen from the above experimental data, the values of VIP and AIP for the H_2O_2 molecule differ greatly, by 11.65 − 10.62 = 1.03 eV. Therefore, it can be expected that the H_2O_2 molecules in the water solution will have an AIP value significantly lower than VIP = 9.95 eV.

In agreement with the authors' assumptions, the data were obtained theoretically on $H_2O_2(H_2O)_n$ clusters, where n = 0–6 [86]. The AIP values calculated using the DFT B2GP-PLYP method for $H_2O_2(H_2O)_n$ clusters with an increase in n from 0 to 6 decrease significantly and are respectively equal to: 10.50, 9.19, 8.56, 8.29, 8.08, 7.94, 7.82 eV, that is, when n goes from 0 to 6 by 10.50 − 7.82 = 2.68 eV [86].

Given the proximity of the two values obtained, it can be assumed that during the transition from the gas phase to liquid water, this decrease in AIP for H_2O_2 (by 2.68 eV) is the same as for H_2O (by 2.70 eV), since it is caused by the same reason − the formation of a system of hydrogen bonds. This means that in liquid water, AIP(H_2O_2) = 10.62 − 2.70 = 7.92 eV, which is very close to the value of AIP = 7.73 eV of the substrate (see the description of the EPR experiment), which in the considered catalytic conditions can be oxidized by the Cu_3Cl_5 molecule on the surface of the white CuCl coating in the presence of an aqueous acetonitrile solution.

Two additional factors that may contribute to the reaction 18 in the considered catalytic conditions may be the intermediate formation of the Cu_3Cl_5...H_2O_2 complex to the SET stage and the tunnel (sub-barrier) method of implementing the SET stage [3].

3.6. Two Chemical Processes Involving Cu_3Cl_5 and Cu_3Cl_4 Molecules

The amount of molecular oxygen evolved under the conditions of experiments 3H and 4D-a is determined by the AIP of the substrate and Cu_3Cl_5 molecules on the surface of the white CuCl coating. In the absence of hydrocarbons, the entire amount of hydrogen peroxide decomposes by reaction 5 and 54.4 mL of O_2 gas is formed. When RH hydrocarbon is added to the reaction mixture, in which AIP(RH) < AIP(H_2O_2), a smaller amount of molecular oxygen is evolved, which is determined by AIP(RH).

At some point in time, reaction 5 stops, and an unreacted amount of H_2O_2 remains in the reaction volume, which can be determined using the straight line in Figure 3H, since the extreme points with AIP of 5 eV (Cu_3Cl_5) and 10.62 eV (H_2O_2) correspond to 100 and 0% of the remaining amount of H_2O_2.

Therefore, the determination of the unreacted amount of H_2O_2, which is one of the traditional stages of catalytic experiments, was not necessary in this case.

Due to the presence of a straight line 3H (the same 4D-a), it is necessary to find answers to two questions: first, why does reaction 5 stop, and second, in what way does AIP(RH) affect the formation of O_2 gas?

Based on visual observations, reaction 5 stops when the yellow complex $Cu_2Cl_4 \cdot 2CH_3CN$ (**16**) stops flowing to the surface of CuCl (**17**), on which Cu_3Cl_5 (**19**) molecules are located.

The influx of complex **16** maintains the necessary concentration of molecules **19**, which are involved in two processes: the formation of O_2 gas and the formation of a crystalline white coating **17**.

Since the molar ratio of products formed by these two processes differs by about two orders of magnitude, these are two parallel processes.

Complex **16** is also consumed in two parallel processes: in the formation of compounds **17** and **18** (reactions 17 and 18, respectively), the ratio of copper atoms in which is 1:2 in the absence of RH hydrocarbons. The amount of precipitating compound **18** depending on the AIP(RH) was not determined.

Based on phenomenological observations, it can be assumed that with a decrease in AIP(RH), the quantity of **17** decreases, and **18** increases accordingly. At AIP(RH) = 5 eV, it should be expected that the copper ions of complex **16** will completely pass into compound **18** since the amount of O_2 gas that is formed due to the influx of complex **16** to surface **17** is zero.

The 3G experiment, in which a white CuCl coating was used as a catalyst, showed that the surface monomeric form of CuCl (**24**), active in reaction 5, over time passed into the crystalline form of CuCl (**17**), which was not active in reaction 5, did not react with H_2O_2 and O_2 was not evolved.

The chemical transformations of different forms of copper occurring on the surface of the white coating can be transmitted by a set of reactions 21–30.

$$CuCl\ (\mathbf{24}) + Cu_2Cl_4 \cdot 2CH_3CN\ (\mathbf{16}) \rightarrow Cu_3Cl_5 + 2CH_3CN \quad (21)$$

$$Cu_3Cl_5 + 2CH_3CN \rightarrow CuCl\ (\mathbf{24}) + Cu_2Cl_4 \cdot 2CH_3CN\ (\mathbf{16}) \quad (22)$$

$$Cu_3Cl_5 + e^- \rightarrow Cu_3Cl_5^{\bullet -} \quad (23)$$

$$Cu_3Cl_5^{\bullet -} \rightarrow Cu_3Cl_5 + e^- \quad (24)$$

$$Cu_3Cl_5^{\bullet -} \rightarrow Cu_3Cl_4 + Cl^- \quad (25)$$

$$Cu_3Cl_4 + e^- \rightarrow Cu_3Cl_4^{\bullet -} \quad (26)$$

$$Cu_3Cl_4^{\bullet -} \rightarrow Cu_3Cl_4 + e^- \quad (27)$$

$$Cu_3Cl_4^{\bullet -} \rightarrow Cu_3Cl_3 + Cl^- \quad (28)$$

$$Cu_3Cl_3 \rightarrow 2CuCl\ (\mathbf{17}) + CuCl\ (\mathbf{24}) \quad (29)$$

$$CuCl\ (\mathbf{24}) \rightarrow CuCl\ (\mathbf{17}) \quad (30)$$

Pairs of reactions 21 and 22, 23 and 24, and 26 and 27 show the reversibility of the processes under consideration. The appearance of complex **16** in the reaction solution by reaction 21 shifts the equilibrium to the right, and in the absence of complex **16**, as, for example, in experiment 3G, by reaction 22, temporary yellowing of the solution occurs, after which O_2 gas begins to be evolved from the surface of CuCl (**17**).

The pair of reactions 23 and 24 is a generalized form of recording reactions 18 and 19, respectively. Since AIP(RH) < AIP(H_2O_2), the smaller the AIP(RH), the more successfully RH competes with H_2O_2 in reactions 23 and 24. The consequence of this is a decrease in the amount of O_2 gas evolved with a decrease in AIP(RH).

The same applies to a pair of reactions 26 and 27. The authors performed additional quantum chemical calculations of the AEA of the compound Cu_3Cl_4 (**31**) and two other

structures (the AEA of Cu_3Cl_3 (**32**) and Cu_2Cl_2 (**33**) is significantly less than 5.02 eV) (Figure 7, Table 2), according to which AEA(Cu_3Cl_4) = 5.32 eV > AEA(Cu_3Cl_5) = 5.02 eV.

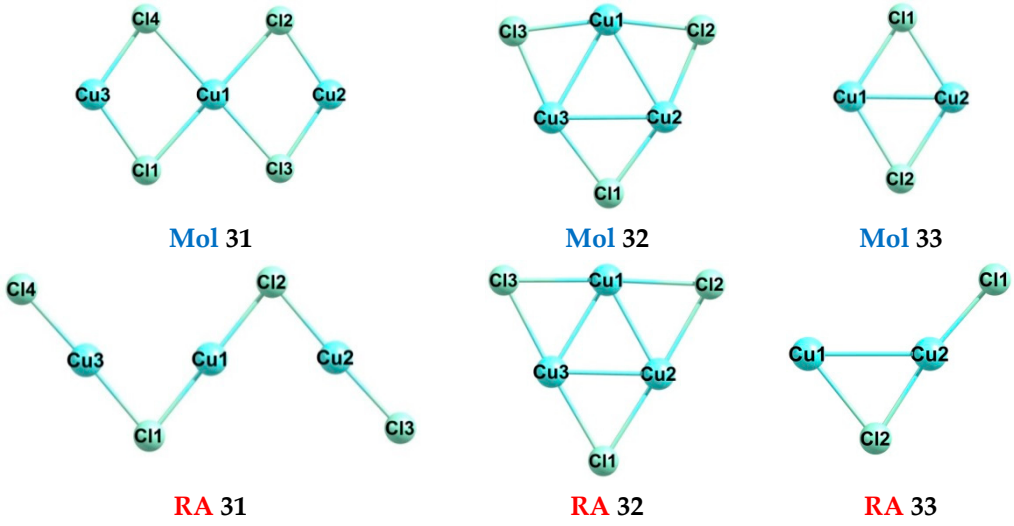

Figure 7. The DFT calculated molecules (**Mol**) and radical anions (**RA**).

Table 2. Experimental and DFT calculated adiabatic electron affinities (AEA, eV) and DFT calculated energies (E, E_h) of molecules (**Mol**) and radical anions (**RA**) of **31**–**33** *.

Formula	No.	Exp.	DFT	A·DFT+B	E(Mol)	E(RA)
Cu_3Cl_4	**31**	-	5.01	5.32	−6761.320975170130	−6761.504989147751
Cu_3Cl_3	**32**	-	0.24	0.78	−6301.307588396459	−6301.316250677407
Cu_2Cl_2	**33**	-	1.37	1.86	−4200.819250735715	−4200.869614232684

* DFT calculated AEA = (E(Mol) − E(RA))·27.2113834; The coefficients: A = 0.9516 and B = 0.5533.

Therefore, if the stage of transfer of the first electron from the substrate by reaction 23 is realized, then reaction 25 will follow, followed by the transfer of the second electron by reaction 26, if this allows the AIP of the ionized substrate or its transformation product. However, if the substrate is H_2O_2, then such a two-electron scheme of substrate oxidation by reactions 31 and 32 cannot be realized, since AIP($HO_2^{\bullet}$) = 11.53 ± 0.02 eV [87] (11.359 ± 0.003 eV [88]) is much larger than AIP(H_2O_2) = 10.62 eV [43,84].

$$Cu_3Cl_5 + H_2O_2 \rightarrow Cu_3Cl_4 + HCl + HO_2^{\bullet} \quad (31)$$

$$Cu_3Cl_4 + HO_2^{\bullet} \text{ —/}\rightarrow Cu_3Cl_3 + HCl + O_2 \quad (32)$$

For energy reasons (negative AEA(H_2O_2) « AEA(Cu_3Cl_5) = 5.02 eV), the SET reaction 33 of electron transfer to H_2O_2, which is a variant of reactions 8 and 13, cannot be realized in the considered catalytic system.

$$Cu_3Cl_5^{\bullet -} + H_2O_2 \text{ —/}\rightarrow Cu_3Cl_5 + HO^{\bullet} + HO^{-} \ (H_2O_2^{\bullet -}) \quad (33)$$

Consequently, reaction 8, which is usually used to ensure the cyclicity of the H_2O_2 oxidation process by ions of transition metals, is not realized in the considered catalytic conditions.

The authors believe that such a role is played by reactions 24 and 27, which ensure the cyclical process of O_2 gas evolution in the pairs of reactions 23, 24, and 26, 27. These pairs

of reactions 23, 24 for Cu_3Cl_5 molecules and 26, 27 for Cu_3Cl_4 molecules are, respectively, a generalization of pairs of reactions 18, 19, and 34, 35.

$$Cu_3Cl_4 + H_2O_2 \rightarrow Cu_3Cl_4^{\bullet -} + H_2O_2^{\bullet +} \quad (34)$$

$$Y^{(\bullet)+} + Cu_3Cl_4^{\bullet -} \rightarrow Y^{(*)} + Cu_3Cl_4 \quad (35)$$

In reactions 19 and 35, a set of possible participants is indicated with the letter Y: H_2O_2, RH, cationic products of their transformations. To understand the processes of O_2 gas evolution, the case of $Y^{\bullet +} = H_2O_2^{\bullet +}...(H_2O_m)_n$ is of the greatest interest, where m = 1, 2, and n = 0–6 (H_2O_2 is individual and in clusters with H_2O and H_2O_2 molecules) [86,89,90].

RC $H_2O_2^{\bullet +}$ can transform into different products before reactions 19 and 35: into $HO_2^{\bullet}$ by reaction 36 [90,91] and into RC $H_2OO^{\bullet +}$ by reaction 37 [92–94], where H_2OO is an oxywater (34) [95,96]. Consequently, $Y^{\bullet +} = H_2OO^{\bullet +}$ can enter into reactions 19 and 35.

$$H_2O_2^{\bullet +} \ldots (H_2O_m)_n \rightarrow HO_2^{\bullet} \ldots H^+(H_2O_m)_n \quad (36)$$

$$H_2O_2^{\bullet +} \rightarrow H_2OO^{\bullet +} \quad (37)$$

In the considered catalytic system, a set of neutral radicals $H^{\bullet}$, $HO_2^{\bullet}$, $HO^{\bullet}$ [97–102], familiar for the generation of H_2 and O_2 gases, can be formed in reactions 38 and 39 of the decay of electronically excited H_2O_2* molecules [103], the source of which are reactions 19 and 35.

$$H_2O_2^* \rightarrow H^{\bullet} + HO_2^{\bullet} \quad (38)$$

$$H_2O_2^* \rightarrow 2HO^{\bullet} \quad (39)$$

The decay of electronically excited H_2OO* molecules by reaction 40 can also be a source of O_2 gas. From a formal point of view, to do this, one needs to enter coefficients 2 in reaction 40 or, while maintaining the general style of presentation of the material adopted in this article, specify reaction 41, which is carried out below.

$$H_2OO^* \rightarrow H_2O + O\ (0.5O_2 \text{ in reaction 5}) \quad (40)$$

$$2O \rightarrow O_2 \quad (41)$$

The participation of Cu_3Cl_4 molecules in reactions 25–28 is a consideration of such possibilities for general reasons. Whether Cu_3Cl_4 molecules participate in reaction 34 is not currently known, since $AEA(Cu_3Cl_4) = 5.32$ eV $\neq AEA(Cu_3Cl_5) = 5.0$ eV, the experimental value determined in experiment 3H, although using DFT calculations, it was found that reaction 34 was possible (Tables 1 and 2).

For the same reason, it is impossible to take as X the participation of three possible molecular forms of copper chlorides at once, based on the fact that arithmetically the average value of AEA(mean) = ($AEA(Cu_3Cl_5) + AEA(Cu_3Cl_4) + AEA(Cu_2Cl_3)$)/3 = (5.02 + 5.32 + 4.70)/3 = 5.01 eV (A·DFT+B, Tables 1 and 2)). The Cu_3Cl_4 and Cu_2Cl_3 molecules are possible, but not proven, products of the chemical transformation of the initiator of the reaction–Cu_3Cl_5. If Cu_3Cl_4 molecules participated in the discussed process of molecular oxygen formation, they would have an energy advantage over the other two forms and would determine a slightly higher (5.32 eV) estimated AEA value.

To an even greater extent, these remarks apply to reactions 25, 26, 28–30, which describe only the formal side of the second process–the formation of a white coating of CuCl (**17**) from the material of complex **16** (reaction 21) arriving at the surface during the reaction, and the monomeric form of CuCl (**24**) located on the surface CuCl (**17**). How this process occurs is not known.

In the gas phase, the geometric structure $(CuCl)_n$ was determined for n =1–4 [104] and calculated theoretically for n =1–12 [105]. These structures can be compared with the geometric structure of CuCl crystals [57–62].

3.7. Evolution of Molecular Hydrogen and Oxygen in an Oscillatory Mode

In some of the conducted experiments (the very first experiment and experiments 2A-a (the same 2C-c), 2B-a,d, 2C-b, 2D-b, 4C-a), the evolution of abnormally large amounts of gas was recorded, which significantly exceeded the maximum volumes of molecular oxygen, theoretically calculated by reaction 5.

This means that in these experiments, along with O_2, H_2 gas was evolved, but in different cases by different reactions. In the very first experiment and experiment 2A-a (the same 2C-c), reaction 4 of the decomposition of H_2O_2 to H_2 and O_2 was realized. In these experiments, the white coating of CuCl (**17**) on the glass walls of the reactor was completely or almost completely absent. Experiments 2B-a,d were not analyzed. In the 2C-b experiment, reaction 2 of the decomposition of H_2O to H_2 and O_2 was realized.

In experiments 2D-b and 4C-a, by the time of the phase of abnormal gas evolution, H_2O_2 and H_2O molecules were in the system, that is, both reactions 4 and 2 could start, respectively. Since the composition of the gases was not analyzed, it is impossible to say exactly in what ratio these two reactions were realized.

Based on the energy effect of reactions 4 ($\Delta E = -0.08$ eV) and 2 ($\Delta E = -3.20$ eV), reaction 4 has a preference. If one compares the energies of homolytic (3.79 and 5.15 eV [7–10], reactions 42 and 43) and heterolytic ($pK_a(H_2O_2) = 11.7 < pK_a(H_2O) = 15.7$, reactions 44 and 45) breaking of the H–O bonds of the H_2O_2 and H_2O molecules, respectively, then reaction 4 is easier to initiate than reaction 2. Therefore, it is most likely that reaction 4 was realized in the considered catalytic conditions with an abnormal gas evolution.

$$H\text{-}O_2H \rightarrow H^{\bullet} + {}^{\bullet}O_2H \quad (42)$$

$$H\text{-}OH \rightarrow H^{\bullet} + {}^{\bullet}OH \quad (43)$$

$$H\text{-}O_2H \rightarrow H^{+} + {}^{-}O_2H \quad (44)$$

$$H\text{-}OH \rightarrow H^{+} + {}^{-}OH \quad (45)$$

Common to all reactions with the phase of the evolution of an abnormal amount of gas was that the abnormal mode was turned on at the moment when the SET mechanism of activation of H_2O_2 molecules by reaction 18 was impossible or turned off. This means that the SET mechanism has the lowest activation energy barrier and the highest reaction rate than other potentially present methods of activating the processes of gas evolution in the system.

Such alternative methods to the SET mechanism are any other schemes that involve the initiation of homolytic or heterolytic breaking of the H–O and O–O bonds of H_2O_2 and H_2O molecules with the formation of a set of particles: $H^{\bullet}$, $HO^{\bullet}$, $HO_2^{\bullet}$, H^+, HO^-, HO_2^- (reactions 42–45). This means that the catalytic forms of copper switch from initiating the SET stage to initiating free radical or ionic particles and their corresponding reactions 42–45.

At the same time, the catalytic forms of copper adsorb the H_2O_2 reagent, generate free radical-like and ionic intermediates from it, stabilize them and ensure the course of reaction stages 4 on the surface copper atoms, adsorb the reaction products (H_2 and O_2), which then pass into the gas phase. Some of these stages have been studied by experimental and theoretical methods for the Cu atom and its cations, CuCl, and $CuCl_2$ molecules in the gas, liquid, and solid phases [106–118].

In the studied catalytic system, several forms of copper were simultaneously present: Cu(0), Cu(I), Cu(II) and, possibly, Cu(III), which could be part of mono-, di-, tri- and so on dimensional formations. Therefore, it is not possible to determine without additional research, which form of copper initiates and how reaction 4 occurs. In the case of initiating the transfer of one hydrogen atom in a generalized form for $(CuCl_m)_n$, where m = 0–3, n = 1–3,..., this reaction 4 can be written as reactions 46 and 47.

$$(CuCl_m)_n + H_2O_2 \rightarrow {}^{\bullet}(CuCl_m)_nH + HO_2^{\bullet} \quad (46)$$

$$^{\bullet}(CuCl_m)_n\text{-}H^{(\delta-)} + {}^{(\delta+)}H\text{-}O_2{}^{\bullet} \rightarrow (CuCl_m)_n + H_2 + O_2 \quad (47)$$

It should be noted that the simplest free radical method proposed by the authors (reactions 46 and 47) is not the only one or the most likely since there are several other possible options for the implementation of reaction 4, which the authors have not tested and therefore will not discuss them further.

Since reaction 4 is the reverse of reaction 3 of the direct synthesis of H_2O_2 from H_2 and O_2, the mechanism of reaction 4 may include, in reverse order, the same composition of key stages determined by experimental and theoretical methods for reaction 3 [18–25,119–123].

The second feature of the abnormal evolution of gases is its oscillatory mode, which was observed not only at 50 °C (see the previous enumeration of experiment numbers) but also at 0 °C (experiment 4E). The authors do not have additional information to formulate general assumptions on how exactly the oscillatory mode of H_2 and O_2 gases evolution is realized in the considered catalytic conditions. However, based on the experience of other authors, one can mention some types of additional experiments that are necessary for such purposes.

In systems containing H_2O_2 molecules and Cu(II) ions, oscillatory reactions were most often recorded by means of measuring pH [124,125], potentiometry [126,127] and chemiluminescence [128,129], as well as using calorimetry [130] and electron spin resonance (ESR) [131]. Oscillations in the potential of a platinum electrode were recorded during the reduction of H_2O_2 both in the presence and in the absence of Cu(II) ions [132–134].

Useful information was obtained by using several methods, for example, by measuring pH and redox potential [135–138], redox potential and chemiluminescence [139], the potential of a platinum electrode, pH, and concentration of O_2 [140].

4. Conclusions

In the $RH/H_2O_2/Cu_2Cl_4{\cdot}2DMG/CH_3CN$ system, where RH is a set of hydrocarbons with the first adiabatic ionization potentials (AIPs, eV) of a wide range, and DMG is dimethylglyoxime (Butane-2,3–dione dioxime), conditions were found in which the evolved gas consisted only of molecular oxygen (normal mode gas evolution) and a mixture of molecular hydrogen and molecular oxygen (abnormal mode of gas evolution).

It was found that the normal mode of gas evolution was initiated by the single electron transfer (SET stage) from H_2O_2 to monomeric Cu_3Cl_5 molecules located on the surface of the white CuCl coating, which was formed on the surface of the glass reactor during the reaction.

It was shown that the stage of the abnormal mode of gas evolution, which proceeded in an oscillatory mode, was activated at the moment when the SET mechanism of activation of H_2O_2 molecules was impossible or turned off.

The boundary between two modes of gas evolution: normal redox and abnormal oscillatory, was determined.

Supplementary Materials: The following supporting information can be downloaded at https://www.mdpi.com/article/10.3390/hydrogen4010006/s1, Table S1: The Charge, Spin state, Energy and XYZ coordinates of all atoms of all structures optimized by the DFT method.

Author Contributions: Conceptualization, I.Y.S.; methodology, I.Y.S.; software, I.Y.S.; validation, A.I.N. and I.Y.S.; formal analysis, A.I.N. and I.Y.S.; investigation (oxidation), A.I.N. and I.Y.S.; investigation (DFT calculations), I.Y.S.; resources, A.I.N. and I.Y.S.; data curation, A.I.N. and I.Y.S.; writing—original draft preparation, I.Y.S.; writing—review and editing, A.I.N. and I.Y.S.; visualization, I.Y.S.; supervision, A.I.N. and I.Y.S.; project administration, A.I.N. and I.Y.S.; funding acquisition, A.I.N. and I.Y.S. All authors have read and agreed to the published version of the manuscript.

Funding: This research was carried out without any financial support.

Institutional Review Board Statement: Not applicable.

Informed Consent Statement: Not applicable.

Data Availability Statement: Not applicable.

Conflicts of Interest: The authors declare no conflict of interest.

References

1. Nikolaidis, P.; Poullikkas, A. A comparative overview of hydrogen production processes. *Renew. Sustain. Energy Rev.* **2017**, *67*, 597–611. [CrossRef]
2. Zhang, L.; Zhou, M.; Wang, A.; Zhang, T. Selective hydrogenation over supported metal catalysts: From nanoparticles to single atoms. *Chem. Rev.* **2020**, *120*, 683–733. [CrossRef] [PubMed]
3. Yu, X.; Tong, Y.; Yang, Y. Activated dissociation of H_2 on Cu(001): The role of quantum tunneling. *arXiv* **2022**, arXiv:2211.06157. [CrossRef]
4. Akhmetov, N.S. *General and Inorganic Chemistry*; Cheighton, H.C., Ed.; Rosinkin, A., Translator; MIR Publishers: Moscow, Russia, 1983.
5. Zhang, Y.P.; Cheng, C.H.; Kim, J.T.; Stanojevic, J.; Eyler, E.E. Dissociation energies of molecular hydrogen and the hydrogen molecular ion. *Phys. Rev. Lett.* **2004**, *92*, 203003. [CrossRef] [PubMed]
6. Martin, J.D.D.; Hepburn, J.W. Electric field induced dissociation of molecules in Rydberg-like highly vibrationally excited ion-pair states. *Phys. Rev. Lett.* **1997**, *79*, 3154–3157. [CrossRef]
7. Ruscic, B.; Wagner, A.F.; Harding, L.B.; Asher, R.L.; Feller, D.; Dixon, D.A.; Peterson, K.A.; Song, Y.; Qian, X.; Ng, C.-Y.; et al. On the enthalpy of formation of hydroxyl radical and gas-phase bond dissociation energies of water and hydroxyl. *J. Phys. Chem. A* **2002**, *106*, 2727–2747. [CrossRef]
8. Ruscic, B.; Pinzon, R.E.; Morton, M.L.; Srinivasan, N.K.; Su, M.-C.; Sutherland, J.W.; Michael, J.V. Active thermochemical tables: Accurate enthalpy of formation of hydroperoxyl radical, HO_2. *J. Phys. Chem. A* **2006**, *110*, 6592–6601. [CrossRef]
9. Chase, M.W., Jr. *NIST-JANAF Thermochemical Table*, 4th ed.; American Chemical Society: Washington, DC, USA, 1998. Available online: http://www.nist.gov/srd/monogr.cfm (accessed on 26 November 2022).
10. Luo, Y.-R. *Comprehensive Handbook of Chemical Bond Energies*, 1st ed.; CRC Press: Boca Raton, FL, USA, 2007. [CrossRef]
11. Cook, B. An introduction to fuel cells and hydrogen technology. *Eng. Sci. Educ. J.* **2002**, *11*, 205–216. [CrossRef]
12. Stambouli, A.B.; Traversa, E. Fuel cells, an alternative to standard sources of energy. *Renew. Sustain. Energy Rev.* **2002**, *6*, 297–306. [CrossRef]
13. Mekhilef, S.; Saidur, R.; Safari, A. Comparative study of different fuel cell technologies. *Renew. Sustain. Energy Rev.* **2012**, *16*, 981–989. [CrossRef]
14. Lu, Y.; Mi, Y.; Li, J.; Qi, F.; Yan, S.; Dong, W. Recent progress in semiconductor-ionic conductor nanomaterial as a membrane for low-temperature solid oxide fuel cells. *Nanomaterials* **2021**, *11*, 2290. [CrossRef]
15. Kumar, S.S.; Himabindu, V. Hydrogen production by PEM water electrolysis—A review. *Mater. Sci. Energy Technol.* **2019**, *2*, 442–454. [CrossRef]
16. Aktar, A.; Ahmmed, S.; Hossain, J.; Ismail, A.B.M. Solution-processed synthesis of copper oxide (Cu_xO) thin films for efficient photocatalytic solar water splitting. *ACS Omega* **2020**, *5*, 25125–25134. [CrossRef]
17. Jakhar, M.; Kumar, A.; Ahluwalia, P.K.; Tankeshwar, K.; Pandey, R. Engineering 2D materials for photocatalytic water-splitting from a theoretical perspective. *Materials* **2022**, *15*, 2221. [CrossRef]
18. Dittmeyer, R.; Grunwaldt, J.D.; Pashkova, A. A review of catalyst performance and novel reaction engineering concepts in direct synthesis of hydrogen peroxide. *Catal. Today* **2015**, *248*, 149–159. [CrossRef]
19. Menegazzo, F.; Signoretto, M.; Ghedini, E.; Strukul, G. Looking for the "dream catalyst" for hydrogen peroxide production from hydrogen and oxygen. *Catalysts* **2019**, *9*, 251. [CrossRef]
20. Ricciardulli, T.; Gorthy, S.; Adams, J.S.; Thompson, C.; Karim, A.M.; Neurock, M.; Flaherty, D.W. Effect of Pd coordination and isolation on the catalytic reduction of O_2 to H_2O_2 over PdAu bimetallic nanoparticles. *J. Am. Chem. Soc.* **2021**, *143*, 5445–5464. [CrossRef]
21. Staykov, A.; Kamachi, T.; Ishihara, T.; Yoshizawa, K. Theoretical study of the direct synthesis of H_2O_2 on Pd and Pd/Au surfaces. *J. Phys. Chem. C* **2008**, *112*, 19501–19505. [CrossRef]
22. Todorovic, R.; Meyer, R.J. A comparative density functional theory study of the direct synthesis of H_2O_2 on Pd, Pt and Au surfaces. *Catal. Today* **2011**, *160*, 242–248. [CrossRef]
23. Tian, P.; Ding, D.; Sun, Y.; Xuan, F.; Xu, X.; Xu, J.; Han, Y.F. Theoretical study of size effects on the direct synthesis of hydrogen peroxide over palladium catalysts. *J. Cat.* **2019**, *369*, 95–104. [CrossRef]
24. Song, X.; Sun, K.; Hao, X.; Su, H.Y.; Ma, X.; Xu, Y. Facet-dependent of catalytic selectivity: The case of H_2O_2 direct synthesis on Pd surfaces. *J. Phys. Chem. C* **2019**, *123*, 26324–26337. [CrossRef]
25. Ranganathan, S.; Sieber, V. Recent advances in the direct synthesis of hydrogen peroxide using chemical catalysis—A review. *Catalysts* **2018**, *8*, 379. [CrossRef]
26. Hiroki, A.; LaVerne, J.A. Decomposition of hydrogen peroxide at water-ceramic oxide interfaces. *J. Phys. Chem. B* **2005**, *109*, 3364–3370. [CrossRef] [PubMed]
27. Tatsuoka, T.; Koga, N. Energy diagram for the catalytic decomposition of hydrogen peroxide. *J. Chem. Educ.* **2013**, *90*, 633–636. [CrossRef]

28. Serra-Maia, R.; Bellier, M.; Chastka, S.; Tranhuu, K.; Subowo, A.; Rimstidt, J.D.; Usov, P.M.; Morris, A.J.; Michel, F.M. Mechanism and kinetics of hydrogen peroxide decomposition on platinum nanocatalysts. *ACS Appl. Mater. Interfaces* **2018**, *10*, 21224–21234. [CrossRef]
29. Anikin, O.V.; Bolotov, A.V.; Minkhanov, I.F.; Varfolomeev, M.A.; Tazeev, A.R.; Chalin, V.V.; Lutfullin, A.A.; Abusalimov, E.M. Factors influencing hydrogen peroxide decomposition dynamics for thermochemical treatment of bottomhole zone. *J. Pet. Explor. Prod. Technol.* **2022**, *12*, 2587–2598. [CrossRef]
30. Chowdhury, S.H.; Ahsan, M.; Kabir, M.H.; Alam, S.S.; Hasnat, M.A. Decomposition of hydrogen peroxide using chemical and catalytic methods: A reactor-based approach. *Asian, J. Chem.* **2022**, *34*, 1263–1268. [CrossRef]
31. Perry, S.C.; Pangotra, D.; Vieira, L.; Csepei, L.I.; Sieber, V.; Wang, L.; Ponce de León, C.; Walsh, F.C. Electrochemical synthesis of hydrogen peroxide from water and oxygen. *Nat. Rev. Chem.* **2019**, *3*, 442–458. [CrossRef]
32. Xia, C.; Back, S.; Ringe, S.; Jiang, K.; Chen, F.; Sun, X.; Siahrostami, S.; Chang, K.; Wang, H. Confined local oxygen gas promotes electrochemical water oxidation to hydrogen peroxide. *Nat. Catal.* **2020**, *3*, 125–134. [CrossRef]
33. Huang, A.; Delima, R.S.; Kim, Y.; Lees, E.W.; Parlane, F.G.L.; Dvorak, D.J.; Rooney, M.B.; Jansonius, R.P.; Fink, A.G.; Zhang, Z.; et al. Direct H_2O_2 synthesis, without H_2 gas. *J. Am. Chem. Soc.* **2022**, *144*, 14548–14554. [CrossRef]
34. Walling, C.; Goosen, A. Mechanism of the ferric ion catalyzed decomposition of hydrogen peroxide. Effect of organic substrates. *J. Am. Chem. Soc.* **1973**, *95*, 2987–2991. [CrossRef]
35. Kremer, M.L. "Complex" versus "free radical" mechanism for the catalytic decomposition of H_2O_2 by ferric ions. *Int. J. Chem. Kinet.* **1985**, *17*, 1299–1314. [CrossRef]
36. Stanbury, D.M. The principle of detailed balancing, the iron-catalyzed disproportionation of hydrogen peroxide, and the Fenton reaction. *Dalton Trans.* **2022**, *51*, 2135–2157. [CrossRef]
37. Mochida, I.; Takeshita, K. Transition metal ions on molecular sieves. II. Catalytic activities of transition metal ions on molecular sieves for the decomposition of hydrogen peroxide. *J. Phys. Chem.* **1974**, *78*, 1653–1657. [CrossRef]
38. Ram, R.N.; Gupta, J.R.P.; Prasad, R.B. Gasometric study of kinetics of decomposition of hydrogen peroxide catalysed by Cu(II). *Indian J. Chem.* **1979**, *17A*, 29–31. Available online: http://nopr.niscair.res.in/bitstream/123456789/51497/1/IJCA%2017A%281%29%2029-31.pdf (accessed on 26 November 2022).
39. Perez-Benito, J.F. Reaction pathways in the decomposition of hydrogen peroxide catalyzed by copper(II). *J. Inorg. Biochem.* **2004**, *98*, 430–438. [CrossRef]
40. Perez-Benito, J.F. Copper(II)-catalyzed decomposition of hydrogen peroxide: Catalyst activation by halide ions. *Mon. Chem.* **2001**, *132*, 1477–1492. [CrossRef]
41. Xing, G.; Pham, A.N.; Miller, C.J.; Waite, T.D. pH-dependence of production of oxidants (Cu(III) and/or $HO^{\bullet}$) by copper-catalyzed decomposition of hydrogen peroxide under conditions typical of natural saline waters. *Geochim. Cosmochim. Acta* **2018**, *232*, 30–47. [CrossRef]
42. Shchapin, I.Y.; Ramazanov, D.N.; Nekhaev, A.I.; Borisov, R.S.; Buravlev, E.A.; Maximov, A.L. One-stage catalytic oxidation of adamantane to tri-, tetra-, and penta-ols. *Catalysts* **2021**, *11*, 1017. [CrossRef]
43. Shchapin, I.Y.; Nekhaev, A.I.; Ramazanov, D.N.; Al-Yusufi, M.; Samoilov, V.O.; Maximov, A.L. Hydrocarbon oxidation depth: $H_2O_2/Cu_2Cl_4{\cdot}2DMG/CH_3CN$ system. *Catalysts* **2022**, *12*, 409. [CrossRef]
44. Svedung, D.H. The crystal structure of copper dimethylglyoxime dichloride. *Acta Chem. Scand.* **1969**, *23*, 2865–2878. [CrossRef]
45. Neese, F. The ORCA program system. *WIREs Comput. Mol. Sci.* **2012**, *2*, 73–78. [CrossRef]
46. Neese, F. *ORCA—An Ab Initio, DFT and Semiempirical SCF-MO Package—Version 3.0.1*; Max-Plank-Institute for Chemical Energy Conversion: Ruhr, Germany, 2013; Available online: https://orcaforum.kofo.mpg.de/ (accessed on 26 November 2022).
47. Chemcraft—Graphical software for visualization of quantum chemistry computations. Available online: https://www.chemcraftprog.com (accessed on 26 November 2022).
48. Megnamisi-Belombe, M.; Novotny, M.A. Superexchange in copper(II) dimers. 1. Synthesis, characterization, and magnetic behavior of the novel di-μ-bromo-bis[bromo(dimethylglyoxime)copper(II)],$[CuBr_2(dmgH)]_2$. *Inorg. Chem.* **1980**, *19*, 2470–2473. [CrossRef]
49. Cozar, O.; Znamirovschi, V.; David, L.; Giurgiu, L.; Zsako, J. ESR investigation of some copper(II)-dioxime-dichloride compounds. *J. Appl. Magn. Reson.* **1992**, *3*, 849–857. [CrossRef]
50. Kitiphaisalnont, P.; Boonyang, U.; Boonperm, K.; Siripaisarnpipat, S. Unexpected formation of copper dimethylglyoxime dimer from the reaction of cuprous chloride and tetradentate buthylene-bridged diiminedioxime ligand. *Chiang Mai J. Sci.* **2015**, *42*, 712–717. Available online: http://epg.science.cmu.ac.th/ejournal/ (accessed on 26 November 2022).
51. Egneus, B. Investigations of dioximes and their metal complexes: A survey of the literature since 1963. *Talanta* **1972**, *19*, 1387–1419. [CrossRef]
52. Rodríguez, M.; Llobet, A.; Corbella, M. A theoretical analysis of how geometrical distortions on $Cu(\mu\text{-}Cl)_2Cu$ dimers influence their electronic and magnetic properties. *Polyhedron* **2000**, *19*, 2483–2491. [CrossRef]
53. Rodríguez-Fortea, A.; Alemany, P.; Alvarez, S.; Ruiz, E. Exchange coupling in halo-bridged dinuclear Cu(II) compounds: A density functional study. *Inorg. Chem.* **2002**, *41*, 3769–3778. [CrossRef]
54. Willett, R.D.; Rundle, R.E. Crystal structure of $Cu_2Cl_4(CH_3CN)_2$, $Cu_3Cl_6(CH_3CN)_2$, and $Cu_5Cl_{10}(C_3H_7OH)_2$. *J. Chem. Phys.* **1964**, *40*, 838–847. [CrossRef]
55. Barnes, J.C. Studies of some complexes of copper(II) halides with organic donors. *J. Inorg. Nucl. Chem.* **1969**, *31*, 95–106. [CrossRef]

56. Liu, C.; Talham, D.R.; Park, J.H.; Čižmár, E.; Meisel, M.W. Ferromagnetic dimer interactions in $Cu_2Cl_4(CH_3CN)_2$. *J. Chem. Phys.* **2004**, *120*, 1140–1141. [CrossRef]
57. Rapoport, E.; Pistorius, C.W.F.T. Phase diagrams of the cuprous halides to high pressures. *Phys. Rev.* **1968**, *172*, 838–847. [CrossRef]
58. Boyce, J.B.; Hayes, T.M.; Mikkelsen, J.C., Jr. Extended-x-ray-absorption-fine-structure investigation of mobile-ion density in superionic AgI, CuI, CuBr, and CuCl. *Phys. Rev. B* **1981**, *23*, 2876–2896. [CrossRef]
59. Schwab, C.; Goltzené, A. Cuprous halides. *Prog. Cryst. Growth Charact.* **1982**, *5*, 233–276. [CrossRef]
60. Graneli, B.; Dahlborg, U.; Fischer, P. Neutron poweder diffraction investigation of γ-and β-copper chloride in the temperature range 8–686 K. *Solid State Ion.* **1988**, *28*, 284–293. [CrossRef]
61. Slack, G.A.; Andersson, P. Pressure and temperature effects on the thermal conductivity of CuCl. *Phys. Rev. B* **1982**, *26*, 1873–1884. [CrossRef]
62. Ahn, D.; Park, S.-H. Cuprous halides semiconductors as a new means for highly efficient light-emitting diodes. *Sci. Rep.* **2016**, *6*, 20718. [CrossRef]
63. Ko, Y.J.; Wang, H.; Pradhan, K.; Koirala, P.; Kandalam, A.K.; Bowen, K.H.; Jena, P. Superhalogen properties of Cu_mCl_n clusters: Theory and experiment. *J. Chem. Phys.* **2011**, *135*, 244312. [CrossRef]
64. Calvi, R.M.D.; Andrews, D.H.; Lineberger, W.C. Negative ion photoelectron spectroscopy of copper hydrides. *Chem. Phys. Lett.* **2007**, *442*, 12–16. [CrossRef]
65. Ho, J.; Ervin, K.M.; Lineberger, W.C. Photoelectron spectroscopy of metal cluster anions: Cu^-_n, Ag^-_n, and Au^-_n. *J. Chem. Phys.* **1990**, *93*, 6987–7002. [CrossRef]
66. Wang, L.S.; Wu, H.; Desai, S.R.; Lou, L. Electronic structure of small copper oxide clusters: From Cu_2O to Cu_2O_4. *Phys. Rev. B* **1996**, *53*, 8028. [CrossRef] [PubMed]
67. Leopold, D.G.; Ho, J.; Lineberger, W.C. Photoelectron spectroscopy of mass–selected metal cluster anions. I. Cu^-_n, n = 1–10. *J. Chem. Phys.* **1987**, *86*, 1715–1726. [CrossRef]
68. Trainham, R.; Fletcher, G.D.; Larson, D.J. One- and two-photon detachment of the negative chlorine ion. *J. Phys. B* **1987**, *20*, L777. [CrossRef]
69. Maier, J.P.; Turner, D.W. Steric inhibition of resonance studied by molecular photoelectron spectroscopy Part 3. Anilines, phenols and related compounds. *J. Chem. Soc. Faraday Trans. 2* **1973**, *69*, 521–531. [CrossRef]
70. Zhelyazkova, B.G. The influence of the solvent on the reaction of cupric chloride with N, N-dimethylaniline. *Inorg. Nucl. Chem. Lett.* **1981**, *17*, 141–145. [CrossRef]
71. Sumalekshmy, S.; Gopidas, K.R. Reaction of aromatic amines with $Cu(ClO_4)$ 2 in acetonitrile as a facile route to amine radical cation generation. *Chem. Phys. Lett.* **2005**, *413*, 294–299. [CrossRef]
72. Sreenath, K.; Suneesh, C.V.; Ratheesh Kumar, V.K.; Gopidas, K.R. Cu(II)-mediated generation of triarylamine radical cations and their dimerization. An easy route to tetraarylbenzidines. *J. Org. Chem.* **2008**, *73*, 3245–3251. [CrossRef]
73. Sreenath, K.; Suneesh, C.V.; Gopidas, K.R.; Flowers, R.A. Generation of triarylamine radical cations through reaction of triarylamines with Cu(II) in acetonitrile. A kinetic investigation of the electron-transfer reaction. *J. Phys. Chem. A* **2009**, *113*, 6477–6483. [CrossRef]
74. Sreenath, K.; Thomas, T.G.; Gopidas, K.R. Cu(II) mediated generation and spectroscopic study of the tris (4-anisyl) amine radical cation and dication. Unusually shielded chemical shifts in the dication. *Org. Lett.* **2011**, *13*, 1134–1137. [CrossRef]
75. Malkondu, S.; Erdemir, S. A triphenylamine based multi-analyte chemosensor for Hg_2^+ and Cu_2^+ ions in MeCN/H_2O. *Tetrahedron* **2014**, *70*, 5494–5498. [CrossRef]
76. Thomas, T.G.; Shekar, S.C.; Swathi, R.S.; Gopidas, K.R. Triazatruxene radical cation: A trigonal class III mixed valence system. *RSC Adv.* **2017**, *7*, 821–825. [CrossRef]
77. Boess, E.; Van Hoof, M.; Birdsall, S.L.; Klussmann, M. Investigating the oxidation step in the $CuCl_2$-catalyzed aerobic oxidative coupling reaction of N-aryl tetrahydroisoquinolines. *J. Org. Chem.* **2019**, *85*, 1972–1980. [CrossRef]
78. Morgante, P.; Dughera, S.; Ghigo, G. Aerobic $CuCl_2$-catalyzed dehydrogenative cross-coupling of tertiary amines. A combined computational and experimental study. *J. Phys. Chem. A* **2019**, *123*, 2796–2814. [CrossRef]
79. Winter, B.; Weber, R.; Widdra, W.; Dittmar, M.; Faubel, M.; Hertel, I.V. Full valence band photoemission from liquid water using EUV synchrotron radiation. *J. Phys. Chem. A* **2004**, *108*, 2625–2632. [CrossRef]
80. Perry, C.F.; Zhang, P.; Nunes, F.B.; Jordan, I.; von Conta, A.; Wörner, H.J. Ionization energy of liquid water revisited. *J. Phys. Chem. Lett.* **2020**, *11*, 1789–1794. [CrossRef]
81. Barth, S.; Oncák, M.; Ulrich, V.; Mucke, M.; Lischke, T.; Slavicek, P.; Hergenhahn, U. Valence ionization of water clusters: From isolated molecules to bulk. *J. Phys. Chem. A* **2009**, *113*, 13519–13527. [CrossRef]
82. Thürmer, S.; Seidel, R.; Winter, B.; Ončák, M.; Slavíček, P. Flexible H_2O_2 in water: Electronic structure from photoelectron spectroscopy and ab initio calculations. *J. Phys. Chem. A* **2011**, *115*, 6239–6249. [CrossRef]
83. Cabral, B.J.C. Dynamics, magnetic properties, and electron binding energies of H_2O_2 in water. *J. Chem. Phys.* **2017**, *146*, 234502. [CrossRef]
84. Ashmore, F.S.; Burgess, A.R. Study of some medium size alcohols and hydroperoxides by photoelectron spectroscopy. *J. Chem. Soc. Faraday Trans. 2* **1977**, *73*, 1247–1261. [CrossRef]

85. Schio, L.; Alagia, M.; Dias, A.A.; Falcinelli, S.; Zhaunerchyk, V.; Lee, E.P.F.; Mok, D.K.W.; Dyke, J.M.; Stranges, S. A Study of H_2O_2 with threshold photoelectron spectroscopy (TPES) and electronic structure calculations: Redetermination of the first adiabatic ionization energy (AIE). *J. Phys. Chem. A* **2016**, *120*, 5220–5229. [CrossRef]
86. Ferreira, C.; Martiniano, H.F.; Cabral, B.J.C.; Aquilanti, V. Electronic excitation and ionization of hydrogen peroxide–water clusters: Comparison with water clusters. *Int. J. Quantum Chem.* **2011**, *111*, 1824–1835. [CrossRef]
87. Foner, S.N.; Hudson, R.L. Mass spectrometry of the HO_2 free radical. *J. Chem. Phys.* **1962**, *36*, 2681–2688. [CrossRef]
88. Tang, X.; Lin, X.; Garcia, G.A.; Loison, J.-C.; Fittschen, C.; Röder, A.; Schleier, D.; Gu, X.; Zhang, W.; Nahon, L. Threshold photoelectron spectroscopy of the HO_2 radical. *J. Chem. Phys.* **2020**, *153*, 124306. [CrossRef] [PubMed]
89. Thompson, W.E.; Lugez, C.L.; Jacox, M.E. The infrared spectrum of $HOOH^+$ trapped in solid neon. *J. Chem. Phys.* **2012**, *137*, 144305. [CrossRef] [PubMed]
90. Pysanenko, A.; Pluhařová, E.; Vinklárek, I.S.; Rakovský, J.; Poterya, V.; Kočišek, J.; Fárník, M. Ion and radical chemistry in $(H_2O_2)_N$ clusters. *Phys. Chem. Chem. Phys.* **2020**, *22*, 15312–15320. [CrossRef]
91. Yamasaki, S.; Tachikawa, H. Intracluster reaction dynamics of ionized micro-hydrated hydrogen peroxide (H_2O_2): A direct ab initio molecular dynamics study. *ACS Omega* **2022**, *7*, 33866–33872. [CrossRef]
92. Del Rio, W.A.; Fortenberry, R.C. Rotational and vibrational fingerprints of the oxywater cation (H_2OO^+), a possible precursor to abiotic O_2. *J. Molec. Spectrosc.* **2019**, *364*, 111183. [CrossRef]
93. Fortenberry, R.C.; Trabelsi, T.; Westbrook, B.R.; Del Rio, W.A.; Francisco, J.S. Molecular oxygen generation from the reaction of water cations with oxygen atoms. *J. Chem. Phys.* **2019**, *150*, 201103. [CrossRef]
94. de Petris, G.; Cartoni, A.; Cipollini, R.; Troiani, A. A novel route to $H_2O_2^{+\bullet}$ ions via direct generation of the oxywater cation $H_2OO^{+\bullet}$. *Int. J. Mass Spectrom.* **2006**, *249–250*, 311–316. [CrossRef]
95. Franz, J.; Francisco, J.S.; Peyerimhoff, S.D. Production of singlet oxygen atoms by photodissociation of oxywater. *J. Chem. Phys.* **2009**, *130*, 084304. [CrossRef]
96. Xu, S.; Jirasek, V.; Lukes, P. Molecular dynamics simulations of singlet oxygen atoms reactions with water leading to hydrogen peroxide. *J. Phys. D Appl. Phys.* **2020**, *53*, 2755204. [CrossRef]
97. Weiss, J. The Free radical mechanism in the reactions of hydrogen peroxide. *Adv. Catal.* **1952**, *4*, 343–365. [CrossRef]
98. Simpson, J.A.; Cheeseman, K.H.; Smith, S.E.; Dean, R.T. Free-radical generation by copper ions and hydrogen peroxide. *Biochem. J.* **1988**, *254*, 519–523. [CrossRef]
99. Hanna, P.M.; Mason, R.P. Direct evidence for inhibition of free radical formation from Cu(I) and hydrogen peroxide by glutathione and other potential ligands using the EPR spin-trapping technique. *Arch. Biochem. Biophys.* **1992**, *295*, 205–213. [CrossRef]
100. Assaf, E.; Fittschen, C. Cross section of OH radical overtone transition near 7028 cm^{-1} and measurement of the rate constant of the reaction of OH with HO_2 radicals. *J. Phys. Chem. A* **2016**, *120*, 7051–7059. [CrossRef]
101. Abd Elhamid, M.H.; Ateya, B.G.; Weil, K.G.; Pickering, H.W. Calculation of the hydrogen surface coverage and rate constants of the hydrogen evolution reaction from polarization data. *J. Electrochem. Soc.* **2000**, *147*, 2148–2150. [CrossRef]
102. Wang, L.; Jiang, J.; Ma, J.; Pang, S.; Zhang, T. A review on advanced oxidation processes homogeneously initiated by copper(II). *Chem. Eng. J.* **2022**, *427*, 131721. [CrossRef]
103. Thiebaud, J.; Aluculesei, A.; Fittschen, C. Formation of HO_2 radicals from the photodissociation of H_2O_2 at 248 nm. *J. Chem. Phys.* **2007**, *126*, 186101. [CrossRef]
104. Hargittai, M.; Schwerdtfeger, P.; Réffy, B.; Brown, R. The molecular structure of different species of cuprous chloride from gas-phase electron diffraction and quantum chemical calculations. *Chem. Eur. J.* **2003**, *9*, 327–333. [CrossRef]
105. Tian, Z.; Cheng, L. First principles study on the structural evolution and properties of $(MCl)_n$ (n = 1 − 12, M = Cu, Ag) clusters. *RSC Adv.* **2016**, *6*, 30311–30319. [CrossRef]
106. Plitt, H.S.; Bär, M.R.; Ahlrichs, R.; Schnöckel, H. [Cu(η^2-H_2)Cl], a model compound for H_2 complexes. Ab initio calculations and identification by IR spectroscopy. *Angew. Chem. Int. Ed. Engl.* **1991**, *30*, 832–834. [CrossRef]
107. Belyung, D.P.; Hranisavljevic, J.; Kashireninov, O.E.; Santana, G.M.; Fontijn, A.; Marshall, P. Laser-induced fluorescence and mass spectrometric studies of the Cu + HCl reaction over a wide temperature range. Formation of HCuCl. *J. Phys. Chem.* **1996**, *100*, 17835–17839. [CrossRef]
108. Mårtensson, P.; Larsson, K.; Carlsson, J.O. Atomic layer epitaxy of copper: An ab initio investigation of the CuCl/H_2 process: I. Adsorption of CuCl on Cu(111). *Appl. Surf. Sci.* **1998**, *136*, 137–146. [CrossRef]
109. Mårtensson, P.; Larsson, K.; Carlsson, J.O. Atomic layer epitaxy of copper: An ab initio investigation of the CuCl/H_2 process: II. Reaction energies. *Appl. Surf. Sci.* **1999**, *148*, 9–16. [CrossRef]
110. Mårtensson, P.; Larsson, K.; Carlsson, J.O. Atomic layer epitaxy of copper: An ab initio investigation of the CuCl/H_2 process: III. Reaction barriers. *Appl. Surf. Sci.* **2000**, *157*, 92–100. [CrossRef]
111. Zhang, L.; Zhou, M.; Chen, M.; Qin, Q. Dioxygen bound to copper and nickel halides: Matrix-isolation FTIR and DFT studies on $ClCu(O_2)$ and $ClNi(O_2)$ molecules. *Chem. Phys. Lett.* **2000**, *325*, 447–452. [CrossRef]
112. Xia, F.F.; Yi, H.B.; Zeng, D. Hydrates of Cu^{2+} and $CuCl^+$ in dilute aqueous solution: A density functional theory and polarized continuum model investigation. *J. Phys. Chem. A* **2010**, *114*, 8406–8416. [CrossRef]
113. Suleiman, I.A.; Mackie, J.C.; Kennedy, E.M.; Radny, M.W.; Dlugogorski, B.Z. Quantum chemical study of copper(II) chloride and the Deacon reaction. *Chem. Phys. Lett.* **2011**, *501*, 215–220. [CrossRef]

114. Zhang, R.; Liu, H.; Wang, B.; Ren, J.; Li, Z. Adsorption and dissociation of O_2 on CuCl(1 1 1) surface: A density functional theory study. *Appl. Surf. Sci.* **2011**, *258*, 408–413. [CrossRef]
115. Kawaguchi, K.; Ito, H.; Kuwahara, T.; Higuchi, Y.; Ozawa, N.; Kubo, M. Atomistic mechanisms of chemical mechanical polishing of a Cu surface in aqueous H_2O_2: Tight-binding quantum chemical molecular dynamics simulations. *ACS Appl. Mater. Interfaces* **2016**, *8*, 11830–11841. [CrossRef]
116. Garg, P.; Rawat, K.S.; Bhattacharyya, G.; Kumar, S.; Pathak, B. Hexagonal CuCl monolayer for water splitting: A DFT study. *ACS Appl. Nano Mater.* **2019**, *2*, 4238–4246. [CrossRef]
117. Wen, J.; Ma, T.; Zhang, W.; van Duin, A.C.; van Duin, D.M.; Hu, Y.; Lu, X. Atomistic insights into Cu chemical mechanical polishing mechanism in aqueous hydrogen peroxide and glycine: ReaxFF reactive molecular dynamics simulations. *J. Phys. Chem. C* **2019**, *123*, 26467–26474. [CrossRef]
118. Wu, P.; Yan, S.; Fang, W.; Wang, B. Molecular mechanism of the mononuclear copper complex-catalyzed water oxidation from cluster-continuum model calculations. *ChemSusChem* **2022**, *15*, e202102508. [CrossRef]
119. Wang, F.; Xia, C.; de Visser, S.P.; Wang, Y. How does the oxidation state of palladium surfaces affect the reactivity and selectivity of direct synthesis of hydrogen peroxide from hydrogen and oxygen gases? A density functional study. *J. Am. Chem. Soc.* **2018**, *141*, 901–910. [CrossRef]
120. Sun, K.; Song, X.; Hao, X.; Su, H.-Y.; Xu, Y. Application of coverage-dependent micro-kinetic study to investigate direct H_2O_2 synthesis mechanism on Pd(111) surface. *Theor. Chem. Acc.* **2020**, *139*, 170. [CrossRef]
121. Chen, L.; Medlin, J.W.; Grönbeck, H. On the reaction mechanism of direct H_2O_2 formation over Pd catalysts. *ACS Catal.* **2021**, *11*, 2735–2745. [CrossRef]
122. Kim, M.-C.; Han, S.S. Electrochemically modeling a nonelectrochemical system: Hydrogen peroxide direct synthesis on palladium catalysts. *J. Phys. Chem. Lett.* **2021**, *12*, 4490–4495. [CrossRef]
123. Han, G.-H.; Lee, S.-H.; Hwang, S.-Y.; Lee, K.-Y. Advanced development strategy of nano catalyst and DFT calculations for direct synthesis of hydrogen peroxide. *Adv. Energy Mater.* **2021**, *11*, 2003121. [CrossRef]
124. Orbán, M.; Epstein, I.R. Chemical oscillators in group VIA: The Cu(II)-catalyzed reaction between hydrogen peroxide and thiosulfate ion. *J. Am. Chem. Soc.* **1987**, *109*, 101–106. [CrossRef]
125. Kurin-Csörgei, K.; Orbán, M.; Rábai, G.; Epstein, I.R. Model for the oscillatory reaction between hydrogen peroxide and thiosulfate catalysed by copper(II) ions. *J. Chem. Soc. Faraday Trans.* **1996**, *92*, 2851–2855. [CrossRef]
126. Gao, J.; Li, Q.; Yang, W.; Liu, X.; Ren, J.; Yang, H.; Deng, H. Determination of L-valine based on an oscillating chemical reaction. *Electroanalysis* **2002**, *14*, 1191–1196. [CrossRef]
127. Pekala, K.; Jurczakowski, R.; Orlik, M. On the interpretation of the potentiometric response of the inert solid electrodes in the monitoring of the oscillatory processes involving hydrogen peroxide. *J. Solid State Electrochem.* **2010**, *14*, 27–34. [CrossRef]
128. Sorouraddin, M.H.; Iranifam, M.; Amini, K. A new enhanced oscillating chemiluminescence system with increased chemiluminescence intensity and oscillation time. *J. Fluoresc.* **2008**, *18*, 443–451. [CrossRef] [PubMed]
129. Gentili, P.L.; Micheau, J.-C. Light and chemical oscillations: Review and perspectives. *J. Photochem. Photobiol. C Photochem. Rev.* **2020**, *43*, 100321. [CrossRef]
130. Jingyan, S.; Yuwen, L.; Jie, L.; Zhiyong, W.; Cunxin, W. Calorimetry studies of a chemical oscillatory system. *J. Therm. Anal. Cal.* **2007**, *90*, 761–767. [CrossRef]
131. Kashima-Tanaka, M.; Tsujimoto, Y.; Yamazaki, M. Quantification of hydroxyl radical generated from the Fe^{2+}-H_2O_2 and Cu^{2+}-H_2O_2 reaction systems by electron spin resonance stop and flow technique. *Int. J. Oral-Med. Sci.* **2002**, *1*, 67–73. [CrossRef]
132. Nakanishi, S.; Mukouyama, Y.; Nakato, Y. Control of the period of an electrochemical oscillation by atomic-or nanometer-scale modifications and structural changes of electrode surfaces in a system of H_2O_2 reduction at Pt electrodes. *J. Electrochem. Soc.* **2001**, *148*, E405. [CrossRef]
133. Mukouyama, Y.; Hara, D.; Kawasaki, H.; Kikuchi, M.; Yamada, Y.; Nakanishi, S. Bifurcation behavior in oscillations during H_2O_2 reduction at Pt electrodes. *ECS Transactions* **2017**, *75*, 113–121. [CrossRef]
134. Okada, H.; Mizuochi, R.; Sakurada, Y.; Nakanishi, S.; Mukouyama, Y. Electrochemical oscillations (named oscillations H and K) during H_2O_2 reduction on Pt electrodes induced by a local pH increase at the electrode surface. *J. Electrochem. Soc.* **2021**, *168*, 076512. [CrossRef]
135. Voeikov, V.L.; Koldunov, V.V.; Kononov, D.S. New oscillatory process in aqueous solutions of compounds containing carbonyl and amino groups. *Kinet. Catal.* **2001**, *42*, 606–608. [CrossRef]
136. Ji, L.; Wang, H.; Hou, X. Complexation amplified pH oscillation in metal involved systems. *J. Phys. Chem. A* **2012**, *116*, 7462–7466. [CrossRef]
137. Jędrusiak, M.; Matyszczak, G.; Orlik, M. On the phase shifts in the dynamics of the H_2O_2–$Na_2S_2O_3$–H_2SO_4–$CuSO_4$ oscillator revealed by comparison of potentiometric responses of different indicator electrodes. *Int. J. Chem. Kin.* **2017**, *49*, 250–258. [CrossRef]
138. Kurin-Csörgei, K.; Poros-Tarcali, E.; Molnár, I.; Orbán, M.; Szalai, I. Chemical oscillations with sodium perborate as oxidant. *Front. Chem.* **2020**, *8*, 561788. [CrossRef]

139. Kiatisevi, S.; Maisch, S. Study of the oscillation and luminol chemiluminescence in the H_2O_2–KSCN–$CuSO_4$–NaOH system. *Chem. Phys. Lett.* **2010**, *499*, 173–177. [CrossRef]
140. Orbán, M.; Kurin-Csörgei, K.; Rábai, G.; Epstein, I.R. Mechanistic studies of oscillatory copper(II) catalyzed oxidation reactions of sulfur compounds. *Chem. Eng. Sci.* **2000**, *55*, 267–273. [CrossRef]